UNIVERSIDADE DE LISBOA
FACULDADE DE CIÊNCIAS
DEPARTAMENTO DE BIOLOGIA VEGETAL

Investigating Cellular and Molecular Neuroendocrine Signalling in the Diabetic Gut

Miguel Ângelo de Freitas Mira

Mestrado em Biologia Molecular e Genética

Dissertação orientada por:
Doutora Inês Guerra Mollet
Professora Doutora Margarida Gama-Carvalho

2021

Agradecimentos

Este culminar da minha vida académica, que foi de longe a fase mais exigente de todas, não teria sido possível sem o auxílio das pessoas que me ajudaram a concretizar este objetivo, ajudando-me nos momentos menos bons e felicitando-me nos mais felizes. Sem todos vocês, esta tese não seria uma realidade, e por isso, estes sinceros agradecimentos são dirigidos a todos vós.

Em primeiro lugar, um especial agradecimento à minha orientadora Doutora Inês Guerra Mollet por toda a companhia, ajuda, exigência, incentivo ao pensamento crítico, liberdade e confiança em mim que permitiu que este trabalho contribuísse para o meu desenvolvimento pessoal. Muito obrigado por toda a paciência que tiveste comigo, e por me dirigires sempre palavras carinhosas.

Um obrigado à Professora Doutora Margarida Gama-Carvalho por ter aceitado tornar-se minha orientadora interna e por me ter auxiliado na construção desta tese.

A todo o grupo de investigação da Professora Doutora Helena Vieira (*Cell Death and Disease*), em particular a Inês, a Cristiana, o Nuno e a Daniela, muito obrigado por me ajudarem a manter a minha sanidade mental quando dava em louco com a falta de resultados. Pela vossa companhia durante os almoços, pelas partilhas de chocolate na hora do café, pelos conselhos dados durante as nossas reuniões ou fora delas, pelo excelente ambiente criado, um especial agradecimento.

Agradeço também à Doutora Maria Paula Macedo e ao seu grupo de investigação (*MEDIR*: *Metabolic Disorders*) pela disponibilização dos murganhos pré-diabéticos e dos reagentes para o IPGTT, à Sara Marques, coordenadora do Biotério de roedores da NMS, pela gentileza em escolher e disponibilizar os murganhos para abate que foram aproveitados para este estudo, à Ana Farinho do departamento de Histologia pela disponibilidade e auxílio prestado durante os cortes intestinais, em particular no manuseamento do crióstato, e ao Telmo Pereira do departamento de Microscopia por toda a ajuda concedida, desde o funcionamento dos microscópios à aprendizagem no ImageJ.

Aos amigos que já me acompanham há anos, Maria, Cláudio e Catarina, muito obrigado por estarem sempre do meu lado durante os bons e maus momentos. Desde os trabalhos de grupo aos jantares improvisados à última hora, passando pelas sessões de jogos, pelas idas à praia ou à piscina, pelas cantorias, ou simplesmente pelos vossos ombros amigos quando mais precisei de desabafar ou de deitar cá para fora a minha frustração, um especial agradecimento a vocês.

À Patrícia e à Margarida, muito obrigado por terem sido de longe o pilar mais fundamental da minha vida académica. À Patrícia, muito obrigado pela companhia nos transportes e por seres a recetora principal dos meus desabafos. À Margarida, muito obrigado pela tua calma, simpatia, companhia, suporte, e também pela casa que tantas vezes me ajudou quando não tinha onde dormir. Às duas, um especial agradecimento pelos risos e gargalhadas, pelas histórias partilhadas nas aulas laboratoriais, pelas sessões de filmes e séries que fizemos e que tanto me ajudaram a distrair quando eu mais precisava, e por nunca terem deixado de estar ao meu lado, mesmo quando posso ser difícil de aturar.

À Buracas, muito obrigado por teres sido a minha primeira amiga nesta jornada universitária, a que ajudou a não me sentir desamparado nos primeiros tempos de Faculdade, e a que esteve sempre preocupada com o meu bem-estar físico e emocional. À Mariana, à Bárbara, à Isidro, à Ana Marta e ao restante *Fac Me*(*r*), à Vanessa, ao Gonçalo, à Catarina, ao Miguel, e aos demais que conheci na FCUL, muito obrigado pelo vosso companheirismo, amizade, e pelo carinho que sempre disponibilizaram.

Por último, e sem dúvida o mais importante, um eterno agradecimento à minha família, em especial os meus avós, tios e primos do lado materno, pelo apoio incondicional que tenho recebido durante toda a minha vida e que, sem ele, não teria sido capaz de ter a força necessária para alcançar os meus objetivos. À minha querida mãe, Maria da Graça, muito obrigado por teres sempre lutado por mim para que eu tivesse sempre o que precisava para concretizar este meu sonho, por teres demonstrado orgulho e carinho por mim, e por acreditares sempre em mim e nas minhas capacidades, mesmo quando eu duvidei que elas existissem. Sem ti, eu não estaria onde estou hoje.

Funding

This study has been supported by funding through a Project Support Grant from the British Society for Neuroendocrinology (BSN), and by Portuguese funds through FCT – Fundação para a Ciência e a Tecnologia (Ministério da Ciência, Tecnologia e Ensino Superior) in the framework of the Applied Molecular Biosciences Unit-UCIBIO (UID/Multi/04378/2019) grant, the Associate Laboratory Institute for Health and Bioeconomy (LA/P/0140/2020), the iNOVA4Health – Programme in Translational Medicine (UID/Multi/04462/2019), and the Life Sciences for a Healthy and Sustainable Future (LA/P/0087/2020).

iNOVA4Health

Abstract

Diabetes mellitus (DM) is a chronic disease characterized by hyperglycaemia and glucose intolerance. By 2019, 463 million people worldwide (9.3%) suffered from this disease. Type 2 diabetes mellitus (T2DM) accounts for about 90% of all DM cases, with higher prevalence in aged populations. This disease is characterized, at early stages (prediabetes), by impaired fasting glucose and glucose intolerance, and after several years, by insulin resistance, hyperglycaemia, and eventually impaired insulin secretion, leading to serious health complications.

Current treatments only serve to regulate hyperglycaemia and attenuate progression of T2DM. However, by chance, remission of T2DM was observed within days after bariatric surgery involving duodenal/jejunal gut bypass, pointing to those bypassed regions as major culprits in its aetiology. Changes in gut hormones and gut microbiome could explain this observed remission, but the molecular mechanisms underlying it remain inconclusive.

Gut signalling in response to ingested nutrients involves enterocytes, diverse enteroendocrine cells (EECs), and networks of enteric glia, intrinsic and extrinsic nerves that communicate with the peripheral and central nervous systems. γ-aminobutyric acid (GABA), the main inhibitory neurotransmitter, is present in enteric nerves and EECs, implicating GABA-mediated neurotransmission in the regulation of physiological functions within the gastrointestinal tract. GABA mediates its effects via GABA receptors, including the heterodimeric and metabotropic $GABA_B$ receptors ($GABA_BR$), whose G protein signalling is regulated by homo-oligomers of auxiliary subunits termed potassium channel tetramerization domains (KCTDs).

$KCTD_8$, $KCTD_{12}$ and $KCTD_{16}$ function specifically with $GABA_BR_2$, regulating downstream intracellular pathways via G protein coupling, including voltage-gated calcium ion channels, potassium ion channels, and adenylyl cyclase. However, the distribution of $GABA_BR_2$ with specific KCTDs in the gut and their role in ageing or T2DM progression is still unknown.

We extracted the proximal small intestine of young, old, and high-fat diet-induced prediabetic (HFD) C57BL/6J male mice, and used proximity ligation assay (PLA) and immunofluorescence (IF), to investigate KCTD proteins colocalized with $GABA_BR_2$, and IF-only, to investigate KCTD expression in non-glial (presumed neural cells) and glial cells, in the interior of intestinal villi.

PLA and IF results showed that expression of $KCTD_8$ and $KCTD_{16}$ colocalized with $GABA_BR_2$ in HFD mice declined 0.4 and 0.6-fold respectively, when compared to mice on a normal chow diet (NCD). However, in old mice, all KCTDs colocalized with $GABA_BR_2$ had a 1.0 to 2.5-fold increase, compared to young mice. These results reveal an age-independent disruption of $KCTD_8$ and $KCTD_{16}$ $GABA_BR$ signalling in prediabetes.

IF studies revealed that glial cells not expressing KCTDs were increased overall in both old and HFD mice, indicating enhanced gut inflammation. In non-glial cells (presumed neural cells), we observed a 50-fold increased expression of $KCTD_{12}$ in prediabetic mice, but a 0.7-fold decrease of $KCTD_{16}$ in old mice. Glial cell expression of all KCTDs studied increased in old mice, but decreased 0.6-fold for $KCTD_{16}$ in prediabetic mice. From these results, we infer that proximal small intestine $GABA_BR$ signalling is disrupted in prediabetes independent of age, with a possible involvement of decreased $KCTD_{16}$-expressing enteric glia, and highlight $KCTD_{12}$ and $KCTD_{16}$ as potential pharmacological targets to study prediabetes prevention.

Keywords: ageing; enteric glia; enteric nervous system; potassium channel tetramerization domain; prediabetes.

Resumo

A glucose é um dos monossacarídeos mais importantes para a vida, uma vez que o nosso organismo a utiliza como uma fonte de energia indispensável ao funcionamento normal dos vários órgãos e tecidos que dela precisam. Para que esse uso aconteça, é necessário que a glucose passe da corrente sanguínea para o interior das células, sendo que esse transporte é possível graças a uma substância química concebida pelo organismo: a insulina. A insulina é uma hormona produzida pelas células β pancreáticas das ilhotas de Langerhans que é libertada das mesmas quando os níveis de "açúcar" na corrente sanguínea se encontram elevados. Contudo, na diabetes mellitus (DM), esta situação está alterada.

A DM é uma doença crónica caracterizada pelo aumento desregulado dos níveis de glucose no sangue, fenómeno designado por hiperglicemia, e pela incapacidade do organismo em transportar toda a glucose proveniente dos alimentos, levando a um desequilíbrio nos seus níveis sanguíneos. Nos últimos dez anos, o impacto do envelhecimento da estrutura etária da população portuguesa (20-79 anos) levou a um aumento de cerca de dois pontos percentuais na taxa de prevalência da DM entre 2009 e 2018, o que equivale a um crescimento de cerca de 16,3%. Mundialmente, em 2019, 463 milhões de pessoas tinham DM (9,3% da população até à data), sendo que 134 milhões se encontravam entre os 65 e os 99 anos (19,4% da população contida nessa faixa etária). Em Portugal, a prevalência nessa faixa etária fixava-se nos 24%. Estima-se que essas prevalências cresçam a um ritmo alarmante, o que leva a que a DM seja considerada uma grande ameaça mundial para a saúde pública.

O tipo mais comum de DM, a DM tipo 2 (T2DM), que ocorre em cerca de 90% da população mundial com DM, e cuja prevalência é mais elevada em indivíduos mais envelhecidos, resulta, numa fase inicial (pré-diabetes), de uma anomalia nos níveis de glucose em jejum e de uma intolerância a este carbohidrato. Após vários anos, as células do nosso organismo ficam incapazes de responder de forma correta à insulina, induzindo-se uma resistência a esta hormona que levará a um aumento nos seus níveis de produção, e eventualmente, à incapacidade das células β em compensar este desequilíbrio. Tudo isto provocará a ocorrência de complicações macrovasculares, tais como doença coronária e hipertensão arterial, e microvasculares, nomeadamente retinopatia e neuropatia, que podem causar complicações severas que diminuirão drasticamente a qualidade e esperança média de vida dos indivíduos com T2DM.

Os tipos de cirurgia bariátrica são divididos em três grupos: 1) os principalmente restritivos, que incluem a banda gástrica ajustável e a gastrectomia vertical, e que diminuem a quantidade de alimentos ingeridos por diminuição do volume gástrico, 2) os principalmente disabsortivos, como a derivação biliopancreática e o *duodenal switch*, em que a perda de peso é altamente eficaz, uma vez que reduzem o trajeto no qual os nutrientes vão ser absorvidos, e 3) os que usam uma combinação de ambas as técnicas, também designados por procedimentos mistos, como é o caso do *bypass* gástrico em Y de Roux (RYGB).

No RYGB, é criada uma pequena bolsa gástrica com cerca de trinta mililitros de capacidade que é ligada ao intestino delgado ao nível do jejuno, pelo que as regiões do intestino delgado proximal (i.e., duodeno e início do jejuno) nunca sofreriam a ação das secreções pancreática e biliar. Contudo, e completamente por acaso, a regressão da T2DM que se observou dias após este *bypass* gástrico colocam em evidência o intestino delgado proximal como um dos principais intervenientes da etiologia desta doença. Modificações dos níveis hormonais, principalmente ao nível do péptido semelhante ao glucagão 1 (GLP-1), e do microbioma intestinal têm sido estudadas para explicar esta regressão, mas os mecanismos moleculares subjacentes permanecem inconclusivos.

Em condições normais, os processos de sinalização ao nível da parede intestinal que ocorrem em resposta a certos nutrientes ingeridos envolvem enterócitos, células enteroendócrinas (EEC's), e uma rede de glias entéricas, nervos intrínsecos e extrínsecos que comunicam com o sistema nervoso central (CNS) e com o periférico. Para que haja propagação do sinal, é necessário que um neurónio pré-sináptico

seja capaz de gerar e propagar um potencial de ação através do seu axónio, transmitindo-o por uma sinapse mediante a libertação de neurotransmissores. Esses neurotransmissores irão potenciar uma reação num neurónio pós-sináptico ou numa célula efetora, tais como as células musculares e a maioria das células exócrinas e endócrinas.

Ao nível do CNS dos mamíferos em desenvolvimento, o principal neurotransmissor inibitório corresponde ao ácido γ-aminobutírico [nome IUPAC: ácido 4-aminobutanoico (GABA)], neurotransmissor esse que se encontra presente nos nervos entéricos e em EEC's intestinais. Como tal, a neurotransmissão mediada pelo GABA considera-se envolvida 1) na regulação das funções fisiológicas ao nível do trato gastrointestinal, e 2) como sendo um mediador enteroendócrino que influencia a função desse trato.

O GABA exerce a sua função através da ligação aos respetivos recetores, podendo os mesmos ser classificados em ionotrópicos ($GABA_A$) ou metabotrópicos ($GABA_B$). Dos dois, a informação relacionada com o recetor $GABA_B$ ($GABA_BR$) é a mais escassa, visto que 1) estes recetores foram dos últimos a ser caracterizados a nível molecular, e 2) apenas dois derivados agonísticos do GABA, baclofeno e ácido γ-hidroxibutirato, são capazes de se ligar ao lado ortostático da estrutura deste recetor. Contudo, os seus efeitos secundários, tais como dormência e tonturas, levam a que a administração destes derivados seja desfavorável em muitos casos de patologia.

A nível molecular, os $GABA_BRs$ consistem em duas subunidades, $GABA_BR_1$ e $GABA_BR_2$, sendo que o $GABA_BR_2$ é também importante para o acoplamento das proteínas G, cuja sinalização é regulada por homo-oligómeros de subunidades auxiliares, aos quais se dá o nome de domínios de tetramerização dos canais de potássio (KCTD's).

$KCTD_8$, $KCTD_{12}$ e $KCTD_{16}$ pertencem ao clado F de uma grande família de vinte e cinco proteínas humanas KCTD que atuam especificamente com os $GABA_BR$, regulando vias intracelulares a jusante via o acoplamento a proteínas G, nomeadamente os canais de iões cálcio dependentes de voltagem, os canais de iões potássio, e o adenilato ciclase. Mais concretamente, as proteínas KCTD interagem com um resíduo de tirosina-902 presente no terminal-C do domínio intracelular da subunidade $GABA_BR_2$. No entanto, a distribuição do $GABA_BR_2$ com estas proteínas específicas ao nível do duodeno e do início do jejuno, assim como o possível papel dessa interação no envelhecimento ou na progressão da T2DM, ainda são desconhecidas.

Neste estudo, procedeu-se à extração do intestino delgado proximal proveniente de murganhos masculinos C57BL/6J que foram usados como modelos de envelhecimento e de pré-diabetes induzida por uma dieta rica em gordura (HFD). Esta região intestinal foi estudada sob a forma de secções do duodeno ou de rolinhos intestinais, secções essas que foram analisadas mediante dois ensaios imuno-histoquímicos: ligação por proximidade (PLA) e imunofluorescência (IF), que permitiram investigar a co-localização das proteínas KCTD com a subunidade $GABA_BR_2$, e apenas IF, para analisar os níveis de expressão dos KCTD ao nível das células não gliais (presumivelmente neurais) e gliais marcadas com a proteína ácida fibrilar glial (GFAP), um dos melhores marcadores para simbolizar a ativação da glia entérica após situações de danos estruturais ou de *stress* ao nível do sistema nervoso entérico. Estas análises imuno-histoquímicas foram efetuadas na porção interior das vilosidades intestinais, à qual se dá o nome de lâmina própria.

Os resultados obtidos por PLA e por IF demonstraram que, nos murganhos HFD, a expressão das proteínas $KCTD_8$ e $KCTD_{16}$ co-localizadas com o $GABA_BR_2$ decresceu na ordem das 0.4 e 0.6 vezes respetivamente, quando comparada com os murganhos alimentados com uma dieta normal (NCD). No entanto, nos murganhos envelhecidos (20 meses de idade), todos os KCTD co-localizados com esta subunidade sofreram um aumento de cerca de 1.0 a 2.5 vezes na sua expressão, quando comparada com os murganhos jovens (4 meses). Estes resultados indicam que a sinalização potenciada pelo $GABA_BR$ e dependente do $KCTD_8$ e do $KCTD_{16}$ sofre uma disrupção independente da idade em casos de pré-diabetes.

Os estudos de IF revelaram que as células gliais que não expressam as proteínas KCTD sofreram um aumento geral da sua expressão em todos os murganhos, o que é indicativo de uma maior inflamação intestinal com a idade e com a pré-diabetes. Nas células não gliais (presumivelmente células neurais), observou-se um aumento de 50 vezes na expressão do $KCTD_{12}$ ao nível dos murganhos HFD, e um decréscimo de 0.7 vezes para o $KCTD_{16}$ nos murganhos envelhecidos. Finalmente, a expressão de todos os KCTD estudados ao nível das células gliais aumentou em todos os murganhos envelhecidos, mas decresceu 0.6 vezes para o $KCTD_{16}$ nos murganhos HFD. A partir destes resultados, podemos inferir que a sinalização mediada pelo $GABA_BR$ ao nível do intestino delgado proximal sofreu uma disrupção independente da idade ao nível dos modelos pré-diabéticos, sendo que a glia entérica, quando co-localizada com o $KCTD_{16}$ (decréscimo nos seus níveis), pode estar envolvida nessa disrupção. Para além disso, o $KCTD_{12}$ em células não gliais, pelo facto de apresentar uma expressão aumentada significativamente em condições pré-diabéticas, pode ser considerado, juntamente com o $KCTD_{16}$, como um potencial alvo farmacológico para estudar a prevenção desta doença crónica.

Palavras-chave: domínios de tetramerização dos canais de potássio; glia entérica; idade; pré-diabetes; sistema nervoso entérico.

Graphical Abstract

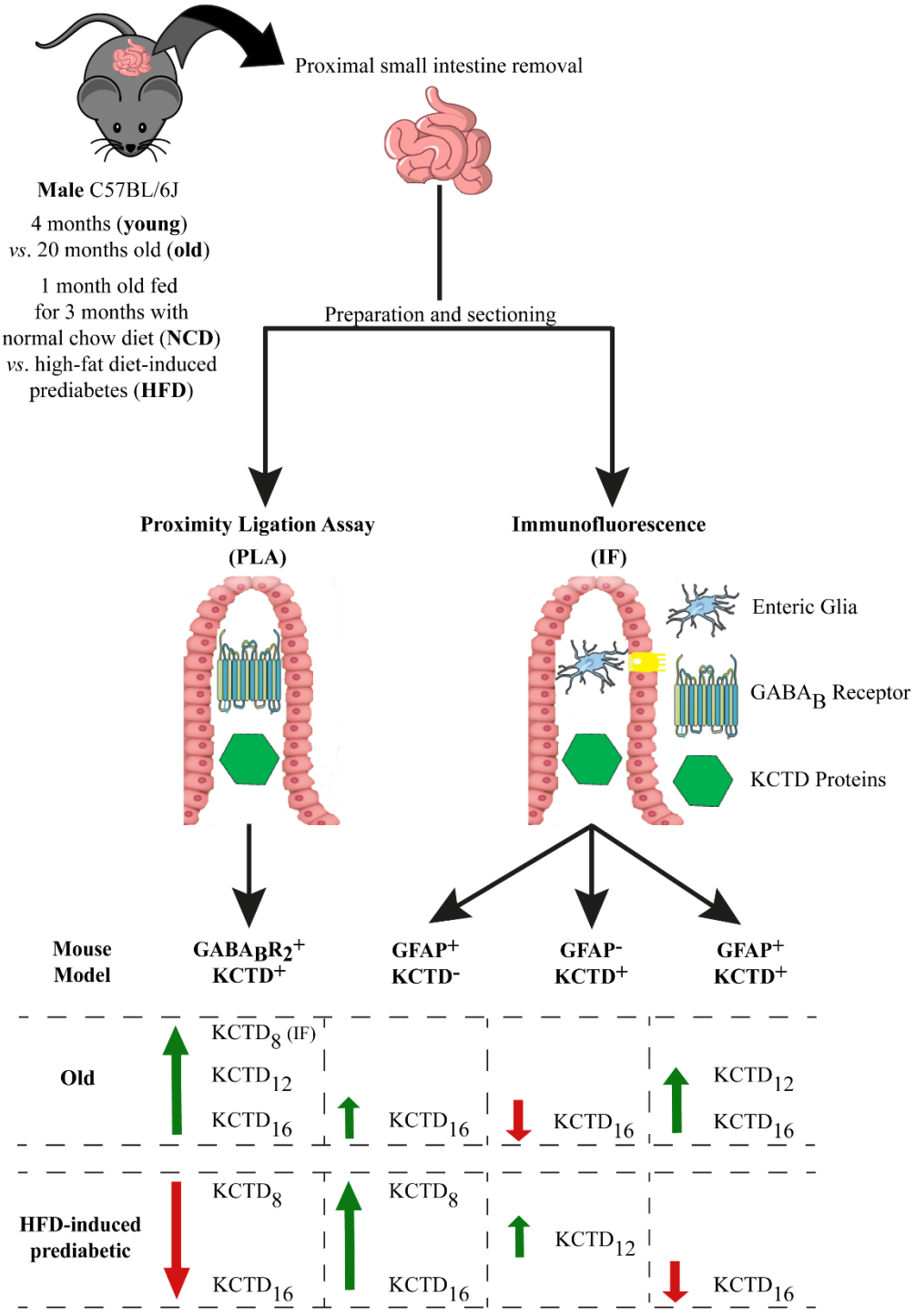

Table of Contents

Index of Figures

Index of Tables

List of Abbreviations, Chemical Compounds, Ions and Proteins

3D – Three dimensional

AMP – Antimicrobial protein

ATP – Adenosine triphosphate

AUC – Area under the curve

BSA – Bovine serum albumin

BTB – Broad-complex, tramtrack, and bric-à-brac domain

Ca^{2+} – Calcium ion

CCK – Cholecystokinin

Cl^- – Chloride ion

CNS – Central nervous system

CO_2 – Carbon dioxide

CTCF – Corrected total cellular fluorescence

DAPI – 4'-6-Diamidino-2-phenylindole

DM – Diabetes mellitus

DNA – Deoxyribonucleic acid

DOB – Date of birth

EEC – Enteroendocrine cell

ENS – Enteric nervous system

FITC – Fluorescein isothiocyanate

GABA – γ-aminobutyric acid

$GABA_AR$ – γ-aminobutyric acid type A ionotropic receptor

$GABA_BR$ – γ-aminobutyric acid type B metabotropic receptor

$GABA_BR_2$ – γ-aminobutyric acid type B metabotropic receptor subunit 2

GAD_{65} – 65 kDa glutamic acid decarboxylase

GDM – Gestational diabetes mellitus

GFAP – Glial fibrillary acidic protein

GHB – γ-hydroxybutyric acid

GI – Gastrointestinal

GIP – Glucose-dependent insulinotropic polypeptide

GIRK – G protein-coupled inwardly-rectifying potassium channel

GLP-1 – Glucagon-like peptide 1

$GLUT_2$ – Glucose transporter type 2

$GLUT_4$ – Glucose transporter type 4

GPCR – G protein-coupled receptor

HFD – High-fat diet

ICQ – Intensity correlation quotient

IDF – International Diabetes Federation

i.e. – *id est* (latin expression for "that is")

IEC – Intestinal epithelial cell

IESC – Intestinal epithelial stem cell

IF – Immunofluorescence

IPGTT – Intraperitoneal glucose tolerance test

K^+ – Potassium ion

KCTD – Potassium channel tetramerization domain

$KCTD_8$ – Potassium channel tetramerization domain containing 8

$KCTD_{12}$ – Potassium channel tetramerization domain containing 12

$KCTD_{16}$ – Potassium channel tetramerization domain containing 16

K_m – Michaelis-Menten constant

mAb – Monoclonal antibody

NCD – Normal chow diet

OCT – Optimal cutting temperature

PA – Picric acid

pAb – Polyclonal antibody

PB – Phosphate buffer

PBS – Phosphate-buffered saline

PFA – Paraformaldehyde

PLA – Proximity ligation assay

PNS – Peripheral nervous system

POZ – Poxvirus and zinc finger domain

PSF – Point spread function

PYY – Peptide tyrosine tyrosine

RBC – Red blood cell

RCA – Rolling-circle amplification

ROI – Region of interest

RYGB – Roux-en-Y gastric bypass

SEM – Standard error of the mean

T1DM – Type 1 diabetes mellitus

T2DM – Type 2 diabetes mellitus

TRITC – Tetramethylrhodamine-isothiocyanate

WHO – World Health Organization

Y_{902} – Tyrosine-902

1. Introduction

1.1. Diabetes mellitus: the fastest growing health crisis in our generation

In 1980, the World Health Organization (WHO) estimated that 108 million people lived with diabetes mellitus (DM), and this number increased fourfold (422 million) by 2014 estimates[1]. More recently, the International Diabetes Federation (IDF) estimated the global prevalence to be equal to 463 million people (9.3% of the global population) by 2019, and they expected this number to increase to 700 million (10.9%) by 2045[2]. More specifically, it has been determined that the prevalence of DM in Portugal (9.9% of the regional population aged 20-79 years old) was slightly higher than the global estimate (8.3%) and the estimate for Europe (8.9%)[2,3]. Therefore, the incidence of DM and its accompanying complications have become one of the most important current public health issues.

In normal conditions, nutrients in food are broken down by our digestive system into smaller molecules that can be absorbed through our digestive tract, and are used by our cells in various catabolic or anabolic processes (glycolysis, glycogenesis, amino acid uptake leading to protein synthesis, and many others). Foods that contain either carbohydrates or sugars will be broken down mainly into glucose, the most important "source of fuel" of all organs in our body, which accumulates in the blood within minutes of food ingestion[4]. The subsequent removal of glucose from the bloodstream can occur due to a hormone produced by the β-cells of the pancreatic islets of Langerhans known as insulin[5].

These β-cells will take up glucose, the most important physiological regulator, through the glucose transporter type 2 channel ($GLUT_2$). This channel allows glucose to pass freely, following a rate of transport that is proportional to the increasing glucose concentration, since it has a high Michaelis-Menten constant (K_m), *id est* (i.e.), a low affinity for glucose (15-20 mM). Therefore, $GLUT_2$ is able to handle large amounts of this carbohydrate, a situation that occurs normally after a meal[6]. Once inside, glucose will be metabolized to adenosine triphosphate (ATP) by a process known as glycolysis, that will, in turn, trigger the secretion of insulin from the β-cells into the bloodstream[7]. When glucose levels are low, the liver, which also has $GLUT_2$ channels, breaks down stored glycogen into glucose (glycogenolysis) to keep its levels within a normal range[8].

Insulin then circulates through the bloodstream to muscle and adipose cells, triggering the "insulin dependent membrane recruitment" of another type of glucose channels [glucose transporter type 4 ($GLUT_4$)]. $GLUT_4$ is present in the cytoplasm of muscle and adipose cells, leading to the removal of glucose from the bloodstream, due to the high affinity of these channels to glucose [Km of 2-5 mM, values that align with the physiological concentration of glucose (5 mM)], and consequent uptake by the cells[6].

DM constitutes a complex metabolic disorder caused primarily due to either a lack of insulin production or an inability of cells/tissues to respond to this hormone, even when its production occurs at a normal level (insulin resistance), leading to impaired fasting glucose levels, and subsequently, its build up in the bloodstream over a prolonged period of time (hyperglycaemia – one of the hallmarks of DM)[9]. Even though other types of DM have been reported, such as gestational diabetes mellitus (GDM) and monogenic DM[2], the following section will only focus on the two main types of DM: type 1 (T1DM) and type 2 diabetes mellitus (T2DM)[9].

1.1.1. Type 1 versus type 2 diabetes mellitus

T1DM, also known as insulin dependent DM, is an autoimmune disease associated with hyperglycaemia and insulin deficiency[9]. This deficiency is primarily caused by a loss of self-tolerance, the destruction of most β-cells, and consequently, an insufficient production of insulin that will result in a glucose imbalance in the body, due to the lack of insulin dependent uptake of this monosaccharide into muscle and adipose cells[6,10]. Although T1DM can appear at any age, occurring in about 5% to 10%

of the world population, this disease primarily affects children and adolescents (almost all cases diagnosed correspond to children aged less than ten years old and most teenagers)[11,12].

On the other side of the spectrum, we have T2DM, also known as insulin independent DM, that corresponds to the most common form of this disease, accounting for approximately 90% to 95% of all DM cases[9]. T2DM is also associated with hyperglycaemia but, unlike T1DM, is characterized by a gradual decline in insulin action (insulin resistance), followed by the inability of the islet β-cells, which usually are responsible for secreting more insulin in order to maintain the glucose homeostasis, to compensate for said resistance, leading to a phenomenon known as "pancreatic β-cell dysfunction"[13,14]. This dysfunction is a key early feature of T2DM that tends to deteriorate throughout disease progression, and is not necessarily a consequence of a preceding loss in β-cell mass[15].

In other words, T2DM is a complex disorder with a complex progression, where the β-cells initially appear to function normally, which means that enough insulin exists in our body that, in normal conditions, would lead to glucose uptake by our muscle and adipose cells[6]. However, due to unknown reasons, glucose remains in the blood for over-extended periods of time after a meal. This will eventually exhaust the pancreas and the individual may become insulin dependent, a situation similar to T1DM[9].

1.1.2. Complications associated with diabetes mellitus and known risk factors

Hyperglycaemia is not the only devastating consequence linked to DM, but it is responsible for a plenitude of long-term vascular complications, as well as long-term dysfunction of several tissues, for example kidneys, eyes, heart and peripheral nerves[16,17]. The chronic elevation of blood glucose levels causes damages to the blood vessels (angiopathy) and leads to several complications that can be grouped under 1) "microvascular disease" (i.e., damages to small blood vessels, namely capillaries, arterioles and venules), that include retinopathy, nephropathy (kidney disease) and neuropathy, or under 2) "macrovascular disease", which results from damages done to the arteries, and may include coronary artery disease, heart attack, stroke, amputation, end stage renal disease and blindness[9,18].

"Diabetic enteropathy", also referred to as diabetes-induced gastrointestinal (GI) complications, corresponds to the modification of the microenvironment contained within the enteric nervous system (ENS) due to the effect of, besides hyperglycaemia, oxidative stress, neuroinflammation, reduced levels of nerve growth factors and structural vascular changes[19,20,21]. "Glucose neurotoxicity" is caused by a fourfold increase in glucose levels (hyperglycaemia) in a persistent or repetitive manner, leading to an extensive intracellular glucose metabolism in the neurons, cellular damage, and ultimately, cellular death[22]. These complications are amongst other DM complications with the highest symptom burden that will cause a negative impact on the individual's quality of life and lifespan.

Of note, it is important to mention that the Global Burden of Disease Study (2019) even identified all forms of DM as the eighth major cause of reduced life expectancy, the third if we just consider all individuals aged 50-74 years old[23]. This could be explained by the fact that age can contribute to an increase in insulin resistance and impaired pancreatic islet function, effects that are primarily associated with adiposity, sarcopenia (muscle atrophy) and physical inactivity. These phenomena will link DM in older adults to a higher mortality, a reduced functional status and an increased risk of institutionalization[24,25,26].

The reasons for the escalating epidemic of DM are multiple, including population ageing (as previously mentioned), economic development and urbanization, ethnicity, unhealthy dietary choices and sedentary lifestyles[27,28,29]. The relationship between genetic and environmental factors in the development of T1DM is not well understood, but many have been proposed and studied[30,31]. Physical and emotional stresses during critical periods of growth and development can lead to 1) overeating, consequently causing obesity, and 2) a negative impact on the body's stress responses, thus affecting metabolic functioning and growth, and potentially inducing an early-onset form of T2DM[32].

Understanding the role of these risk factors is important for developing clear and effective strategies for improving global health, i.e., for diminishing the high prevalence of this chronic disease.

1.2. The relationship between the intestinal epithelial cells and the enteric nervous system

The intestinal epithelium consists of a highly dynamic single layer of cells organized into crypts and villi that form the luminal surface of both the small and large intestine of the GI tract. It is considered the largest of the body's mucosal surfaces, covering approximately 400 square meters of surface area. This surface is continuously renewed through a process of cell division, maturation and migration led by pluripotent intestinal epithelial stem cells (IESCs) that reside in the base of crypts[33].

This epithelium is formed by several cell types, including secretory intestinal epithelial cells (IECs) such as goblet cells and Paneth cells. These cells secrete mucins (heavily glycosylated proteins that provide a medium for facilitating molecular exchanges between the epithelium and the environment) and antimicrobial proteins (AMPs), in order to establish a physical and biochemical barrier that promotes the exclusion of bacteria from the epithelial surface[34,35].

A third set of secretory IECs, called enteroendocrine cells (EECs), are arguably the most important cells of the intestinal epithelium, given that they represent a link between the central and enteric neuroendocrine systems, and have been considered the "chemosensors in the intestinal epithelium"[33,36]. In the GI tract, enterochromaffin cells, a specific type of EECs, are the major sources of serotonin, a neurotransmitter that is considered "integral" for the ENS, since it has been shown to modulate ENS development and neurogenesis, motility, inflammation and epithelial development[37,38,39].

EECs also produce insulinotropic peptide hormones that control metabolism by targeting several tissues involved in food intake, absorption, nutrient disposal and assimililation[40]. These hormones, known as anorexigenic hormones (cause loss of appetite), such as glucose-dependent insulinotropic polypeptide (GIP) from the enteroendocrine K cells and glucagon-like peptide 1 (GLP-1) from enteroendocrine L cells, are released by their respective cells following food ingestion, and act on their respective receptors to amplify glucose-dependent insulin secretion[14,41,42]. It is important to note that, in the duodenum and jejunum, EECs only have a turnover time of ten days, as estimated from thymidine labelling studies[43].

The ENS is considered the "brain of the gut", given that it constitutes a complex network responsible for controlling GI motility, exocrine and endocrine secretions, nutrient uptake, blood flow, and immune and inflammatory processes[44]. This network is formed by two main plexuses known as myenteric (Auerbach's) and submucosal (Meissner's)[45]. The myenteric plexus increases the tone of the gut and the velocity and intensity of contractions (peristaltic waves), which can be orchestrated by extrinsic and intrinsic nerves, while the submucosal plexus is involved mainly with local conditions of the gut lumen, and controls local secretion and absorption[37,46].

It has been shown previously, resorting to three dimensional (3D) electron microscopy, that enteroendocrine I and L cells producing two anorexigenic hormones, cholecystokinin (CCK) and peptide tyrosine tyrosine (PYY) respectively[41,42], revealed an axon-like basolaterally located process named neuropod. The neuropod extends towards the ENS and enteric glia due to the presence of neurofilaments in its structure, and provides a direct communication between the EECs and the networks of enteric glia, intrinsic and extrinsic nerves that communicate with the peripheral (PNS) and central nervous systems (CNS)[47,48]. This entero-neuroendocrine communication is made by using both hormones and neurotransmitters in response to ingested nutrients and other molecules, and may be essential for the regulation of glucose homeostasis and the switch from gluconeogenic (fasting) to the glycolytic (fed) state upon feeding. However, it could be affected in patients with DM, but this hypothesis has yet to be proven.

1.2.1. Understanding GABA and its role as a neurotransmitter

For neurons to send messages throughout the body, they need to be able to communicate with one another to transmit signals. However, neurons are not simply connected to one another. At the end of each one, a tiny gap called synapse exists, and to communicate with the "target" cell, the signal needs to be able to cross this small distance (synaptic cleft). This occurs through a process known as synaptic neurotransmission, where signalling molecules, known as neurotransmitters, are released by the axon terminal of a neuron (presynaptic neuron) and bind to or react with the receptor on the dendrites of the postsynaptic neuron. These neurotransmitters are usually stored in synaptic vesicles clustered close to the cell membrane of the presynaptic neuron, and are only released in response to the depolarization induced by a threshold action potential or graded electrical potential[49,50].

Neurotransmitters can be classified by their function into three different types: 1) excitatory, meaning they are responsible for increasing the likelihood that the neuron will fire an action potential; 2) inhibitory, which corresponds to the type of neurotransmitters that decrease the likelihood of that action potential being fired; 3) modulatory, often referred to as neuromodulators, that are capable of affecting a larger number of neurons at the same time across a large area, in a slow-acting manner[51]. When it comes to the inhibitory neurotransmitters, the most prominent one in the developmentally mature mammalian CNS corresponds to GABA, and therefore, it plays a key role in modulating neuronal activity[52].

GABA is located throughout the GI tract, in enteric nerves and in EECs, which implicate it as both a neurotransmitter and an endocrine mediator of function of this tract[53]. Besides that, this chemical molecule colocalizes with insulin in pancreatic islet β-cells, given that its production occurs within these cells through the catalysis of glutamate to GABA and carbon dioxide (CO_2) by 65 kDa glutamic acid decarboxylase (GAD_{65}), in concentrations like those encountered in the CNS[54]. This colocalization will make it so that GABA will co-secrete with insulin and stimulate the glucose inhibition of glucagon secretion (peptide hormone responsible for raising the concentration of glucose and fatty acids in the bloodstream, and as such, it counteracts the effects induced by insulin)[55].

It has been shown that expression of GAD_{65}, and consequently elevated GABA levels in β-cells, resulted in impaired first-phase insulin secretion and DM in transgenic mice[56], an observation that is in agreement with results proposing an inhibitory role for GABA on insulin secretion in the perfused rat pancreas[57]. However, it has also been shown that GABA can promote the replication and survival of β-cells and the conversion of α- to functional β-cells, inducing an increase in circulating human insulin and a reduction of glucagon levels that may lead to new treatments for DM[58,59]. These contrasting observations elucidate an importance in clarifying exactly what is the role of GABA in T2DM aetiology, and whether its levels are increased, or decreased, in mice subjected to a high-fat diet (HFD).

1.2.2. KCTD and $GABA_BR$: an important association

In vertebrates, GABA acts at inhibitory synapses in the brain by binding to specific transmembrane receptors in the plasma membrane of both pre- and postsynaptic neuronal processes. These receptors can be of two different classes: 1) γ-aminobutyric acid type A ionotropic receptors ($GABA_AR$), in which the receptor is part of a ligand-gated ion channel complex allowing the flow of negatively charged chloride ions (Cl^-) into or out of the cell in a fast-acting way (depending on the resting potential), and therefore, affect fast synaptic transmission in the CNS[60]; 2) γ-aminobutyric acid type B metabotropic receptors ($GABA_BR$), that are G protein-coupled receptors (GPCRs) that regulate opening or closure of positively charged ion channels [mainly potassium (K^+) or calcium ion (Ca^{2+})] in a slow-acting manner, via its linkage to heterotrimeric G proteins and through second messengers[52,61].

The active site of $GABA_AR$ has been associated to the binding site for GABA and several drugs,

for instance muscimol, gaboxadol and bicuculline, and there is reported evidence of an existence of different allosteric binding sites that modulate its activity indirectly and are also targeted by several drugs, namely benzodiazepines, barbiturates, ethanol and picrotoxin[62,63,64]. However, the known information regarding $GABA_BR$ is not as detailed. This is due to the fact that these receptors were one of the last major neurotransmitter receptors to be characterized at a molecular level[65]. In fact, only two GABA derivatives, baclofen and γ-hydroxybutyric acid (GHB), which bind to the orthostatic site of $GABA_BR$, have recently been acknowledged as possible drugs to target this GPCR. Despite this, these selective receptor agonists may be responsible for causing severe adverse effects, such as sedation, tolerance and muscle relaxation, and as such, have limited use in clinical practice[52].

Targeting multiprotein receptor complexes, rather than receptors directly, is a promising concept in drug discovery. This is particularly relevant for $GABA_BR$, a complex that is expressed in almost all neurons and glial cells of the CNS, and therefore, plays a prominent role in many brain functions, like learning and memory formation, and disease, where its dysfunction could lead to some severe neurological disorders, namely epilepsy, schizophrenia, obsessive compulsive disorder and cognitive deficits[52,66]. Much of this functional diversity is believed to arise from their interactions with a large repertoire of intracellular receptor-associated proteins, such as potassium channel tetramerization domains (KCTDs), which stabilize the G protein at the receptor and influence effector K^+ and Ca^{2+} channels[67,68,69].

KCTDs 8, 12, 12b (not found in humans) and 16 correspond to cytosolic proteins belonging to clade F of the twenty-five human KCTD family that interact with an intracellular region of the γ-aminobutyric acid type B metabotropic receptor subunit 2 ($GABA_BR_2$) C-terminus. This interaction occurs within a tyrosine-902 residue (Y_{902}) contained within the cytoplasmic tail of $GABA_BR_2$ via a conserved N-terminal broad-complex, tramtrack, and bric-à-brac domain (BTB), also denoted as poxvirus and zinc finger domain (POZ), leading to the formation of a tetrameric structure[69,70,71]. The fact that these domains are most similar in terms of amino acid sequence to the T_1/BTB domains that mediate tetramerization of voltage-gated K^+ channel subunits to form functional channels explains how these proteins acquired their official name[72].

It has been shown previously that several KCTD tetrameric auxiliary subunits confer subtype specificity on $GABA_BRs$, modulating its agonist potency and pharmacological/kinetic properties in distinct ways[69,73], and generating a fast ($KCTD_{12}$) or slow ($KCTD_8$ and $KCTD_{16}$) desensitizing currents[68]. A previous report has also showcased $GABA_BR$ in the gut with an unknown functional distribution and association with KCTD auxiliary subunit subtypes[69]. These observations present opportunities for the discovery of drugs that target individual receptor subtypes and would allow more specific therapeutic interference with $GABA_BR$-mediated signalling. The disruption of the auxiliary subunits $KCTD_8$, $KCTD_{12}$ and $KCTD_{16}$ may be related to T2DM aetiology, but this is a conclusion that is yet to be proven valid.

1.3. Remission of type 2 diabetes mellitus: the Roux-en-Y gastric bypass

Roux-en-Y gastric bypass (RYGB), the most commonly performed weight-loss surgery, involves the creation of a small pouch (approximately thirty millilitres in volume) from the stomach and its direct connection to the small intestine. After this procedure, swallowed food will go straight from that small pouch into the distal small intestine, bypassing the duodenum and early jejunum, and consequently, changing the pattern of food absorption, as well as the food-stimulated release of gastric hormones, since the proximal small intestine never sees food again[74].

RYGB, on the earlier stages of its execution, was normally performed in obese individuals to achieve weight loss. However, completely by chance, this procedure has proven effective in inducing a profound effect on glucose metabolism in subjects with T2DM. Consequences linked to RYGB include

a decreased insulin resistance and fasting glucagon concentrations, an improved β-cell function (occurring within days after surgery), an increase in the secretion levels of GLP-1, and even a remission of T2DM in rates reportedly as high as 75% to 85%. All these phenomena occurred before any signs of weight loss were displayed, although RYGB also achieves a sustained mean weight loss of 30% to 40%[75,76].

Even though changes in gut hormones and/or its microbiome have been studied to explain T2DM remission after RYGB[77,78,79], the molecular mechanisms underlying this remission, as well as the decrease in insulin resistance, remain incompletely understood, showing that not much progress has been made to aid our understanding of the causes of T2DM. Despite that, the simple fact that this duodenal/jejunum bypass leads to this remission puts a spotlight on the proximal small intestine as a possible root cause of T2DM aetiology and its role in glucose homeostasis.

1.4. Major goals and aim of this study

The overarching goal is to study GABAergic signalling disruption in the proximal small intestine of prediabetic mouse models, to identify pharmacological targets of autonomic and neuroendocrine signalling in the gut that can be further investigated to achieve medical remission of T2DM. In this study, we focus specifically on the G protein-coupled heterodimeric and metabotropic $GABA_BR$.

To achieve this, we observed $GABA_BR$ distribution and their auxiliary KCTD subunits in the prediabetic gut and in gut extracted from young and old mice, resorting to confocal and widefield microscopy (essential due to the complexity of the proximal small intestine) and image analysis software. We expect to 1) determine a functional distribution and association between the different KCTDs with $GABA_BR_2$, and 2) quantify the differences in localization and spatial relationships of the $GABA_BR_2$ auxiliary KCTD subunits relative to enteric glial and non-glial cells, using glial fibrillary acidic protein (GFAP).

We will focus our work on the early stages of T2DM, also referred to as prediabetes, because, at this stage, major damages to the pancreas have not yet occurred, and it is possible to achieve DM remission.

2. Materials and Methods

2.1. Experimental models

All experimental procedures were performed at the rodent facility of NOVA Medical School and according to the Portuguese (Decree-Law number 113/2013 of the 7th of August) and European regulations (Directive 2010/63/EU) that rule the use of animals in research.

All studies performed followed the principle of the three Rs – replacement, reduction, and refinement – to 1) use methods which avoid or replace the use of animals, and reduce the number of animals used per experiment, and 2) look for methods that minimise any form of suffering and improve animal welfare.

Mice in general are a very good model to study T2DM because 1) much that has been learned from mouse models is translatable to human patients, due to the genetic homology between the two species, and 2) T2DM and the murine HFD-induced prediabetes are complex diseases with complex and overlapping pathogenic mechanisms[14].

For this study, C57BL/6J male mice were obtained from in-house breeding of mice originally purchased from Charles River Laboratories (JAX Mice Strain). They were selected based on the previous observations and also because these mice, when placed on a HFD, show a predisposition to develop this form of non-insulin dependent pathology. However, they do not become overly diabetic, and as such, they are considered a powerful model for prediabetes[80].

All mice selected for this study were male because they tend to develop a more severe and consistent phenotype compared to female mice placed on the same diet[81].

2.2. Housing conditions and changes in glucose homeostasis

Young (n = 7) and old mice (n = 13) were housed in either individual or grouped plastic cages, depending on their date of birth (DOB), and were maintained in an environmental temperature of 22 ± 2ºC, relative humidity of 30% to 70%, and a 12:12 hour light:dark cycle, with access to normal chow diet (NCD) and free access to water. Body weight was measured on the day of their dissection and gut retrieval using a scale. Blood glucose levels were determined on the same day through the FreeStyle Precision Neo blood glucose meter (Abbott), with the mouse blood being retrieved through a small cut done perpendicularly to the tip of the tail's direction (the blood flow could be increased by gently massaging the tail's tip-wards[82]). It is important to make sure that the mice remain as calm as possible, so that their glucose levels are not affected by stress[32].

The cohort of 18 weeks old NCD-fed (n = 5) and HFD-fed mice (n = 5) were kept under the same conditions described above as to temperature, humidity, light:dark cycle and free access to water. However, they were also subjected to an intraperitoneal glucose tolerance test (IPGTT), a robust screening test that allows us to infer how well the mice's cells can uptake glucose from bloodstream. Therefore, this test will be indicative of insulin secretion and its posterior effect on metabolism[82].

Briefly, for the prediabetic cohort, mice from 5-6 weeks old were kept on a control NCD that was changed every Thursday, while in parallel, prediabetic mouse models had access to a HFD (D12331, Research Diets) for 12 weeks (each mouse should eat about 2 grams per day) that was changed every Tuesday and Friday. After those 12 weeks, 10 mL of 20% glucose solution were diluted in physiological serum, and 200 µL of glucose were administered via intraperitoneal injection (0.1 mL/10 g body weight). Blood glucose was measured before IPGTT and 15, 30, 60, 90, and 120 minutes after by applying a drop of free-flowing blood on a COUNTOUR® NEXT ONE blood glucose meter test strip. Between measurements, the mice were allowed to rest in their home cages, with unlimited access to water, to minimize the effects of stress[32].

To determine whether glucose tolerance was observed, the area under the curve (AUC) was calculated using the trapezoid method, as described by Andrikopoulos *et al*.[83].

2.3. Preparation and sectioning of proximal small intestine for longitudinal histological analyses

The murine intestinal tract consists of a long convoluted tubular structure with a narrow diameter, a very thin wall, and a delicate mucosa, which makes it a difficult organ system to be studied by histological analyses, given that rapid fixation *in situ*, or organ removal without careful dissection, could lead to poor post-fixation tissue handling and limited options for high quality histological assays. The small intestine, comprised of three functionally distinct units – duodenum, jejunum and ileum – can undergo rapid autolysis, sloughing of epithelium, and possible villus contraction immediately after death, factors that could be misinterpreted as genuine pathological changes[84]. Therefore, after weighting the mice and measuring their blood glucose levels, the process of tissue fixation should be done with the objective of minimizing the time taken between the animal's death and the removal of the tissue of interest.

Young and old mice were subjected to a technique that has been described previously as adapted "Swiss roll"[85]. In summary, after mice were euthanized by cervical dislocation, the abdomen was opened and 15 centimetres of small intestine (starting from the stomach) were removed and kept on ice. The gut was cleaned gently with phosphate-buffered saline (1X PBS, pH 7.4) by squirting it with a micropipette to dislodge digesta, prevent autolysis, and keep the gut section moist. A steel rod wetted with 1X PBS was gently placed through the gut section to hold it flat, and after cutting the stomach, the section was placed onto a filter paper and cut open along the length of the intestine with a razor. Once the steel rod was removed, the gut section was once again washed gently with 1X PBS, and one more filter paper was put on top of it, forming a "sandwich". This "sandwich" was then relocated into a box filled with 4% paraformaldehyde (PFA, A3813, PanReac AppliChem)/0.1% picric acid (PA, 251049, PanReac AppliChem) in 1X PBS to fix tissues overnight at 4ºC.

The next day, the "sandwich" was removed from the PFA/PA solution and was placed onto a 30% sucrose (S9378, Sigma-Aldrich) in 1X PBS solution for cryoprotection, which was kept at 4ºC for 48 hours. Afterwards, the gut section was removed from the "sandwich" and was rolled gently with the help of forceps, pinning it through its centre after it was complete. The gut roll was then placed on warmed (37ºC) gelatin solution [15% sucrose, 7.5% gelatin from porcine skin (G2500, Sigma-Aldrich) in 1X PBS] contained within a little slide box that was then put on ice to solidify the solution. Once it solidified, a small cube that contained gelatin solution and the gut roll (± 1 cm^3) was cut, fixed to an identification card with optimal cutting temperature compound (OCT, 12678646, Fisher Scientific), kept on ice until OCT compound solidified, and then snap-frozen in isopentane (126470250, Enzymatic) placed on dry ice (- 78ºC).

NCD and HFD mice were subjected to the exact same treatment, but instead of rolling the gut sections, the proximal small intestine was divided into duodenum [and its segments (D_1 to D_4)] and jejunum, according to previous reports showcasing their location and how to distinguish them[86,87].

The gut cubes were then sectioned longitudinally on the Leica CM3050 S cryostat by placing a bed volume of OCT compound on its mounting block, and allowing it to freeze in the cryostat chamber (- 25ºC). Once the cubes had reached its optimal cutting temperature, 20 µm roll sections (for young and old mice) and 12 µm duodenal sections (in the case of NCD and HFD mice) were placed onto a glass 1.5H thickness cover glass (630-2187, Van Waters and Rogers International) and were stored at 4ºC until further use. As for the remainder of the gut cubes, they were stored at - 80ºC, allowing multiple sectioning processes at different time periods.

2.4. Immunohistochemical assays

In this study, two different kinds of immunohistochemical assays were performed: 1) proximity ligation assay (PLA) in $GABA_BR_2$ and KCTD double-staining studies (except for $KCTD_8$ staining in NCD and HFD mice), and 2) immunofluorescence (IF) for GFAP and KCTD double-staining assays.

2.4.1. Proximity ligation assay

PLA, also referred to as Duolink® PLA technology, was developed and first described by Fredriksson and colleagues in 2002, and consists of a powerful tool that allows *in situ* detection of proteins, protein modifications and protein interactions, with high specificity and sensitivity. Protein targets can be readily detected and localized with single molecule resolution in unmodified tissues[88].

In the direct PLA method, the one selected for this study, two primary antibodies raised in different species are used to detect two unique protein targets. A pair of oligonucleotide-labelled secondary antibodies that contain a unique deoxyribonucleic acid strand (DNA – PLA probes, one PLUS and one MINUS) then binds to the primary antibodies. Next, hybridizing connector oligos join the PLA probes only if they are less than 40 nanometres away from each other, and ligase forms a closed, circular DNA template that is required for rolling-circle amplification (RCA) of circular DNA molecules. The PLA probe then acts as a primer for a DNA polymerase, which generates concatemeric sequences during RCA. This leads to an 1000-fold amplified signal that is still tethered to the PLA probe, allowing its localization. Lastly, labelled oligos hybridize to the complementary sequences within the amplicon that are then visualized and quantified as discrete spots (PLA signals) by microscopy image analysis[89,90].

Gut rolls of proximal small intestine from young and old mice and gut duodenal sections from NCD and HFD mice were first washed with 0.1 M phosphate buffer (PB) at 37ºC, to remove all gelatin, and incubated with Duolink® blocking solution for 1 hour at 37ºC (1 drop, or approximately 40 µL to each roll/section). After discarding it, the rolls/sections were incubated overnight at 4ºC with a primary antibody consisting of Duolink® antibody diluent, anti-mouse monoclonal $GABA_BR_2$ antibody (mAb, 1:200, NBP2-37281, Novus Biologicals) and anti-rabbit polyclonal $KCTD_8$ (pAb, 1:50, NBP1-86327, Novus Biologicals), $KCTD_{12}$ (1:50, 15523-1-AP, Proteintech®), or $KCTD_{16}$ antibody (1:100, NBP2-30652, Novus Biologicals).

The next day, the cover glasses were incubated at 37ºC for 1) 1 hour with PLA probe solution containing Duolink® antibody diluent, donkey anti-rabbit PLUS (1:5) and anti-mouse MINUS PLA probes (1:5), 2) 30 minutes with ligation solution containing Duolink® ligase (1:40, 1U/µL) and 1X ligation buffer, and 3) 100 minutes in the dark with amplification solution containing Duolink® polymerase (1:80, 10U/µL) and 1X amplification buffer. Between incubations, the cover glasses were washed several times with Duolink® wash buffer A.

After the amplification process, the cover glasses, kept in the dark, were washed with 1X and 0.01X Duolink® wash buffer B, mounted with Duolink® PLA mounting media with 4'-6-diamidino-2-phenylindole (DAPI) to stain the nuclei, sealed around the edges with nail polish, and stored at 4ºC overnight.

2.4.2. Immunofluorescence

IF is a microscope-based technique used to detect specific target antigens by using antibodies labelled with fluorochromes. In this study, indirect IF was performed, in which a primary unlabelled antibody binds to the target and is then recognized by the secondary antibody that is fluorophore-labelled against the Fc portion of the primary antibody[91].

Proximal small intestinal gut rolls from young and old mice and gut duodenal sections from

NCD and HFD mice were first washed with 0.1 M PB at 37ºC, to remove all gelatin, and incubated with block/perm buffer [0.5% bovine serum albumin (BSA, A6003, Sigma-Aldrich) and 0.1% saponin (47036, Sigma-Aldrich) in 1X PBS] for 1 hour at room temperature. After discarding it, the rolls/sections were incubated overnight at 4ºC with a primary antibody (approximately 40 µL to each roll/section) consisted of block/perm buffer, anti-mouse mAb GFAP (1:100, AB_2109791, BioLegend®) and anti-rabbit pAb $KCTD_8$ (1:50), $KCTD_{12}$ (1:50), or $KCTD_{16}$ (1:100).

The next day, the cover glasses were washed with block/perm buffer and incubated in the dark with the secondary antibodies for 2 hours at room temperature. The secondary antibodies used, diluted in block/perm buffer, were Alexa Fluor 488 donkey anti-rabbit (1:1000, A21206, Thermo Fisher Scientific) and Alexa Fluor 594 donkey anti-mouse (1:500, A21203, Thermo Fisher Scientific).

After washing with block/perm buffer and with 0.1 M PB, all samples were stained with Fluoromount-G™ mounting media with DAPI (00-4959-52, Thermo Fisher Scientific) to stain the nuclei, sealed around the edges with nail polish, and stored at 4ºC overnight.

2.5. Image analysis

Images were acquired in a Zeiss LSM 710 Confocal Microscope, except for the images obtained from NCD and HFD mice duodenal sections double-stained with $GABA_BR_2$ and $KCTD_8$ primary antibodies, which were acquired in a Zeiss Axio Imager Z2 Widefield Microscope. Independently of the form of image acquisition, all were analysed with ImageJ software, following the steps illustrated in Table 6.1 (Tables in Appendices).

To make a more accurate proportion of the protein expression levels, we must account for background noise given off by unspecific binding of primary or secondary antibody dye that results in imaging noise, which can vary from image to image. When this is done, it is called the corrected total cellular fluorescence (CTCF), a parameter that can be determined by the following equation (**1**):

$$\text{CTCF} = \text{Integrated density} - [\text{area of selected region of interest (ROI)} \times \text{mean n = 5 background noise readings}] \quad \textbf{(1)}$$

2.5.1. Colocalization assays

Spatial colocalization between two distinctly fluorescence-labelled molecular species (proteins, in most cases) is a common question in optical microscopy. To visualize it, we usually resort to a simple overlay between the different pseudo-coloured channels, leading to the presence of pixels with a different coloration. For example, “green” and “red” channels will give rise to “yellow” hotspots in places where the ROI is present in the exact same pixels on both channels. However, this form of “direct” analysis is still susceptible to the limits of microscope resolution, which implies that an overlap of fluorescence does not necessarily mean that colocalization exists[92].

In this study, we performed a quantitative evaluation of colocalization resorting to two distinct coefficients: 1) Pearson’s correlation coefficient, chosen over Manders’ coefficient because it is a very quick, simple, thoroughly characterized, robust measure that works particularly well for individual cells (ROI) and for images with no/few background noise, and 2) Li’s correlation coefficient, also known as intensity correlation quotient (ICQ), given that, out of all the intensity correlation coefficient-based analyses, it is the one that allows a more readily identifiable showcase of absence of colocalization[92,93].

Following the steps exemplified in Table 6.1, the colocalization analyses were performed on GFAP and KCTD double-stained proximal small intestinal sections, as well as in duodenal sections from NCD and HFD mice double-stained with $GABA_BR_2$ and $KCTD_8$ primary antibodies, by the standards indicated in Table 6.2 (Tables in Appendices).

The results were analysed as described in Table 2.1:

Table 2.1: **Positive**, **negative**, **and inconclusive colocalization analyses based on Pearson and Li's correlation coefficients**.

Possible results	Meaning
Pearson's correlation coefficient ≥ 0.5 Li's correlation coefficient ≥ 0.2	Positive correlation ROI colocalizes in both channels
0.0 ≤ Pearson's correlation coefficient < 0.5 Li's correlation coefficient close or equal to 0.0	Inconclusive results Not accounted for in our analyses
Pearson's correlation coefficient < 0.0 Li's correlation coefficient < 0.0	Negative correlation The respective ROI is positive for only one of the channels

2.5.2. Image deconvolution

Optimal image acquisition on any sort of image analysis, but especially for colocalization, relies mainly on the limits of optical resolution. In that sense, confocal microscopy is a better approach for image acquisition due to the presence of a pinhole that will eliminate out-of-focus light from the detector, allowing an improvement of about 30% of the lateral resolution of the image. In other words, the images obtained in a confocal microscope will not be as "blurred" as ones taken in a widefield microscope[94].

This "blurriness" is due to the diffraction of light, i.e., the light originating from one point in the sample is not at all detected at a single pixel, but it is detected over several pixels and *z*-slices. This process, known as convolution, will define the point spread function (PSF).

The PSF, which varies depending on the wavelength of light and on the numerical aperture of the objective, has an hourglass-like shape due to the axial symmetry along the *z*-axis associated with the overall diffraction of light. This will alter the "perfect" image of the Airy disc, generating an "artefact" that appears elongated in the *z*-axis like a rugby ball[94,95].

To solve this problem, NCD and HFD mice duodenal sections double-stained with $GABA_BR_2$ and $KCTD_8$ primary antibodies were subjected to a computationally intensive image processing technique known as deconvolution, the process of reversing the optical distortion that takes place. This procedure was performed on Huygens Remote Manager (https://huygens.i3s.up.pt/) and involved the parameters stipulated on Table 6.3 (Tables in Appendices).

2.6. Statistical analysis

Normalization is necessary to be able to compare between images or samples. In this specific case, two variables were considered as "normalization variables": the area of the interior portion of the villus (i.e., lamina propria) and the number of nuclei contained within the same region. However, a linear regression between them has shown that both dependent variables have a strong relationship between them [$R^2 = 0.9744$ – Figure 6.1 in Figures (Appendices)], allowing us to choose between either one as our "normalization variable".

The statistical analyses were carried out using GraphPad Prism 8.0.1 (GraphPad Software). Data from ageing and HFD-related changes in glucose metabolism were plotted as mean ± standard error of the mean (SEM) of at least 5 mice. Data from PLA and IF studies were plotted as mean CTCF normalized to the area of the lamina propria (easier to determine than the number of nuclei) ± SEM of replicates. The assays were performed with, at least, 10 villi analysed per mice (when possible and otherwise indicated). The statistical significance was evaluated using an unpaired t-test with Welch's correction, and the differences were considered statistically significant at *p*-value (hereby denoted as *p*) ≤ 0.05 and borderline significant at $p \leq 0.1$.

3. Results

3.1. Ageing and prediabetes-related changes in glucose metabolism

To understand if ageing has any influence on glucose metabolism, we subjected young (4 months old) and old C57BL/6J male mice (20 months old) to a NCD for the time they were kept in their respective cages. Then, we measured their body weight and blood glucose levels at the time of their death (small intestine removal). We observed that, even though body weight was significantly increased ($p \leq 0.05$) in old mice (30.87 ± 0.530 g) when compared to young ones [28.70 ± 0.746 g – Figure 3.1 (A)], no signs of impaired fasting glucose were found, as shown in Figure 3.1 (B) (old: 180.7 ± 9.680 mg/dL; young: 173.7 ± 12.30 mg/dL).

This allowed us to infer that, even though ageing is one of the main risk factors for the development of T2DM, abnormal glucose metabolism associated with it is not a necessary component, placing these mice as age models, but not as prediabetic models.

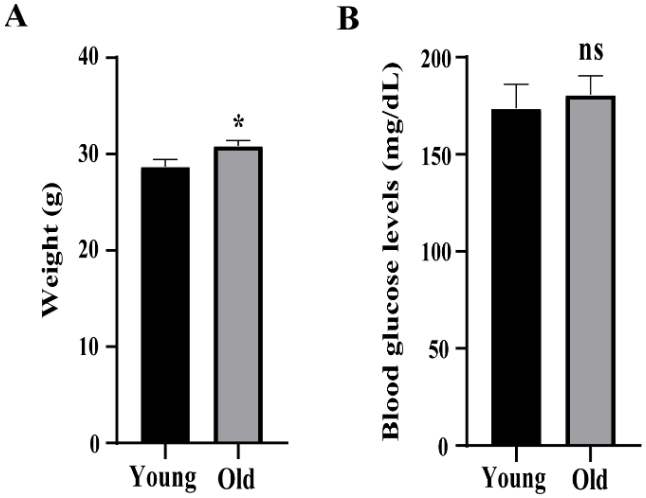

Figure 3.1: **Body weight and blood glucose levels of young and old C57BL/6J male mice**. Mice were fed with NCD throughout their lifetime. Body weight (**A**) and blood glucose levels (**B**) were monitored at the time of their small intestine removal. Data are expressed as mean ± SEM from n = 7 young (4 months old) and n = 13 old (20 months old) mice. Statistical analyses were performed by unpaired t-test with Welch's correction. ns: not significant, *$p \leq 0.05$.

Young mice fed with a HFD for 12 weeks had significantly increased ($p \leq 0.001$) total body weight by an average of 38% when compared to NCD-fed mice [NCD: 24.98 ± 0.576 g; HFD: 34.58 ± 1.150 g – Figure 3.2 (A)]. Blood glucose levels were on average 67% higher in HFD (1893 ± 53.65 mg/dL) than in NCD mice [1132 ± 37.76 mg/dL – Figure 3.2 (B)], while mean blood glucose AUC during IPGTT was 77% higher in HFD mice as well [NCD: 23793.0 ± 2190.69 mg/dL x min; HFD: 42103.5 ± 2251.79 mg/dL x min; $p \leq 0.001$ – Figure 3.2 (C)].

These results show that HFD mice had slight impaired fasting glucose (time point 0 minutes) and impaired glucose tolerance, confirming these mice as models of prediabetes.

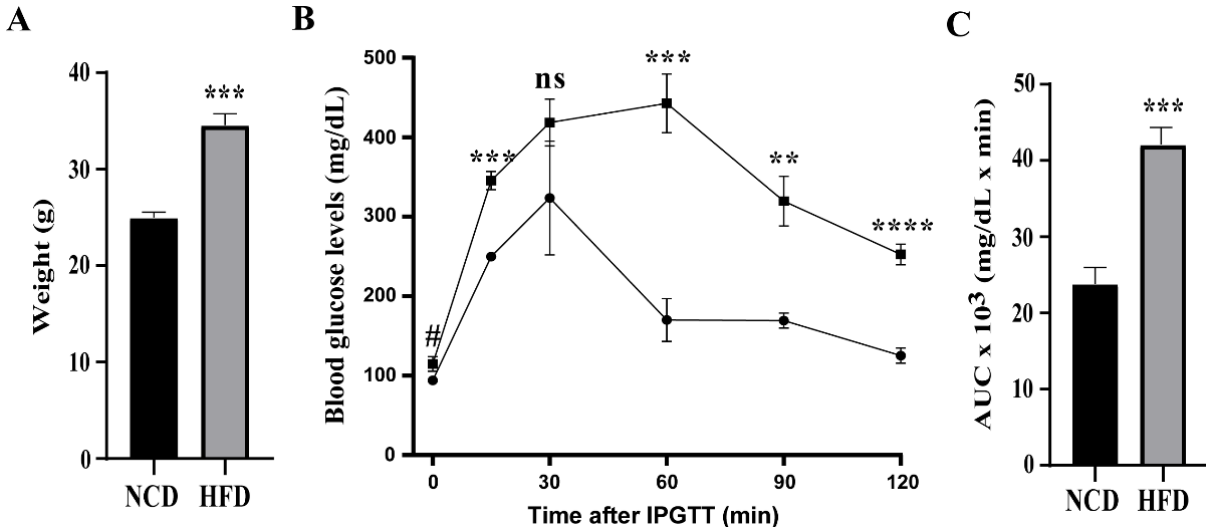

Figure 3.2: **Body weight**, **fasting glucose and IPGTT in NCD and HFD C57BL/6J male mice**. Mice raised in normal housing conditions were fed with either NCD or HFD (prediabetes) for 12 weeks. Mice body weight was determined (**A**), and afterwards, glucose (0.1 mL/10 g) was injected intraperitoneally. 15 minutes later, blood samples were collected in specific time intervals (15, 30, 60, 90 and 120 minutes), and blood glucose levels evolution was measured by a glucometer. The dark circles (●) illustrate the mean blood glucose levels observed in n = 5 NCD mice, while the dark squares (■) refer to the mean blood glucose levels in n = 5 HFD mice (**B**). (**C**) AUC of glucose tolerance assay, as assessed by the trapezoid method. Data are expressed as mean ± SEM. Statistical analyses were performed by unpaired t-test with Welch's correction. ns: not significant, #$p \leq 0.1$, **$p \leq 0.01$, ***$p \leq 0.001$, ****$p \leq 0.0001$.

3.2. Autofluorescence of proximal small intestinal sections and its impact on immunohistochemical assays

To disclose the effect that ageing and prediabetes might have on the functional distribution and association between the different KCTDs with $GABA_BR_2$, or in the localization and spatial relationships of the $GABA_BR_2$ auxiliary KCTD subunits relative to enteric glial cells, it is important to guarantee that we are aware of possible confounding false positive results that may jeopardize our actual findings.

One of the main problems facing immunofluorescent imaging of tissues is autofluorescence. In this case, we noticed that the main source of confounding autofluorescence came from erythrocytes or red blood cells [RBCs – Figure 3.3 (A)]. Since these cells are present in blood vessels and are easily identifiable by their shape and lack of nuclei [Figure 3.3 (B)], they were readily removed from our analyses.

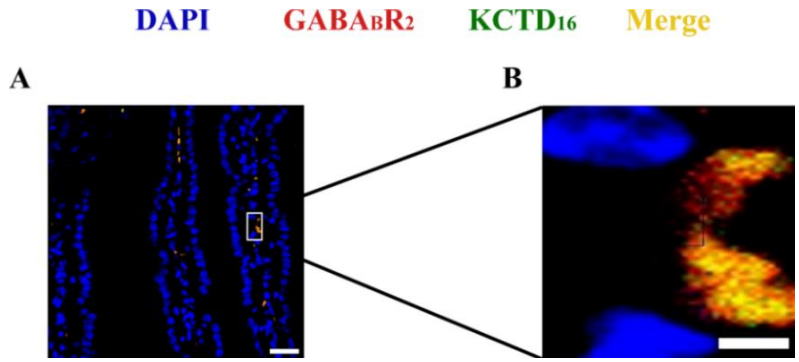

Figure 3.3: **The confounding effect of erythrocytes on double-labelled immunohistochemical assays in frozen sections of proximal small intestine**. In the proximal small intestine, many bright "green" and "red" fluorescence spots were distributed along its surface and were localized in the same structures ("yellow" in **A**), but they were not observed when exposed to the DAPI filter (**B**). Due to their shape and to previous notions that mature erythrocytes lack nuclei, we concluded that those autofluorescence spots were emitted from erythrocytes. **B** corresponds to a 5x magnified image of several erythrocytes (boxed in **A**). **Scall bars**: 25 µm (**A**), 15 µm (**B**).

3.3. Effect of ageing or prediabetes on the expression of $GABA_BR_2$ coupled to KCTD proteins

Since $GABA_B$ signalling is controlled by auxiliary subunits named KCTDs, mainly $KCTD_8$, $KCTD_{12}$ and $KCTD_{16}$, we aimed to infer if ageing or prediabetes can disrupt this tight regulation. Therefore, a PLA was performed on proximal small intestinal sections from young versus old mice, and a cohort of 12 weeks old NCD versus HFD-fed mice. An IF double-staining assay of $GABA_BR_2$ and $KCTD_8$ was also done on NCD and HFD mice, and the expression of $GABA_BR_2$ colocalized with any KCTD protein was determined.

It is important to note that, in PLA, a positive result means that the PLA probes are less than 40 nanometres apart, allowing their hybridization and identification as "yellow" spots in fluorescence imaging, while in IF studies, colocalization was considered when Pearson and Li's correlation coefficient were within the values indicated on Table 2.1.

First, we considered the expression of $GABA_BR_2$ colocalized with $KCTD_8$, and we were able to determine an age-related statistically significant increase (2.478-fold, $p \leq 0.001$) on that expression [old: 4.484 ± 0.751; young: 1.289 ± 0.182 – Figure 3.4 (A) and 3.4 (C)]. HFD had the opposite effect, i.e., it induced a statistically significant decrease [NCD: 1.447 ± 0.163, HFD: 0.747 ± 0.086 when we consider the normalized mean CTCF obtained on the "red" channel (- 0.483-fold, $p \leq 0.001$); NCD: 0.803 ± 0.096 (45.3% of total ROI), HFD: 0.525 ± 0.069 (44.8%) for the normalized mean CTCF obtained on the "green" channel (- 0.345-fold, $p \leq 0.05$) – Figure 3.4 (B) and (D)].

When the expression of $GABA_BR_2$ colocalized with $KCTD_{12}$ was analysed, we obtained very similar results, in the sense that ageing induced a statistically significant increase (1.218-fold, $p \leq 0.01$) on that expression [old: 3.824 ± 0.630; young: 1.724 ± 0.218 – Figure 3.5 (A) and 3.5 (B)], while HFD showed a decreasing trend [NCD: 0.627 ± 0.169; HFD: 0.352 ± 0.115 (- 0.439-fold) – Figure 3.5 (A) and 3.5 (C)].

These conclusions were also alike when we took into account $GABA_BR_2$ colocalized with $KCTD_{16}$, as ageing induced a statistically significant increase (2.538-fold, $p \leq 0.001$) on that expression [old: 1.565 ± 0.307; young: 0.442 ± 0.082 – Figure 3.6 (A) and 3.6 (B)], while HFD had the opposing effect [NCD: 0.265 ± 0.047; HFD: 0.115 ± 0.027 (- 0.564-fold, $p \leq 0.01$) – Figure 3.6 (A) and 3.6 (C)].

Overall, these observations allowed us to infer that prediabetes may be associated with disrupted $GABA_BR$ signalling dependent of $KCTD_8$ and $KCTD_{16}$ and independent of age.

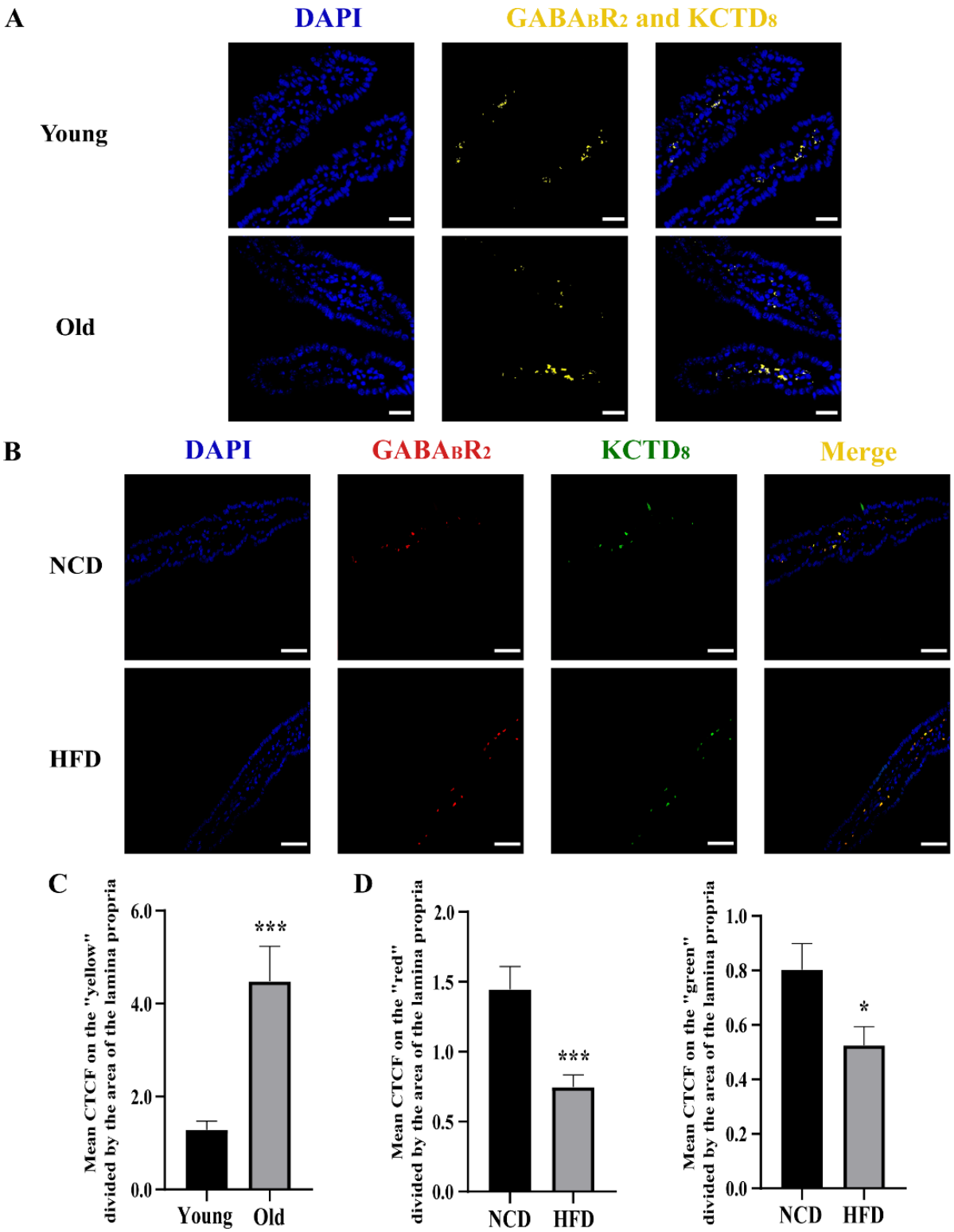

Figure 3.4: **$GABA_BR_2$ colocalized with $KCTD_8$ on proximal small intestinal sections from C57BL/6J male mice**. (**A**) PLA analysis (40x objective lens) in young (4 months old) or old (20 months old) mice. PLA was performed with anti-$GABA_BR_2$ and anti-$KCTD_8$ primary antibodies, and their colocalization was detected by the presence of "yellow" bright spots. Cell nuclei were stained with DAPI ("blue"). **Scale bars**: 25 µm. (**B**) IF images (40x objective lens) of NCD and HFD (prediabetes) mice. Cell nuclei were also stained with DAPI ("blue"). $GABA_BR_2$ expression is indicated by "red" fluorescence, while "green" fluorescence corresponds to $KCTD_8$. Possible positive $GABA_BR_2$ colocalized with $KCTD_8$ appears as "yellow" fluorescence. **Scale bars**: 100 µm. (**C**-**D**) Quantification of the expression of $GABA_BR_2$ colocalized with $KCTD_8$ in PLA (**C**) or IF studies (**D**) by CTCF normalized to the area of the lamina propria. All data are expressed as mean ± SEM and were obtained from (**C**) 138 villi analysed in n = 3 young (95 villi) and n = 2 old mice (43 villi), and from (**D**) 69 villi in n = 2 NCD (34 villi) and n = 3 HFD mice (35 villi). Statistical analyses were performed by unpaired t-test with Welch's correction. *$p \leq 0.05$, ***$p \leq 0.001$.

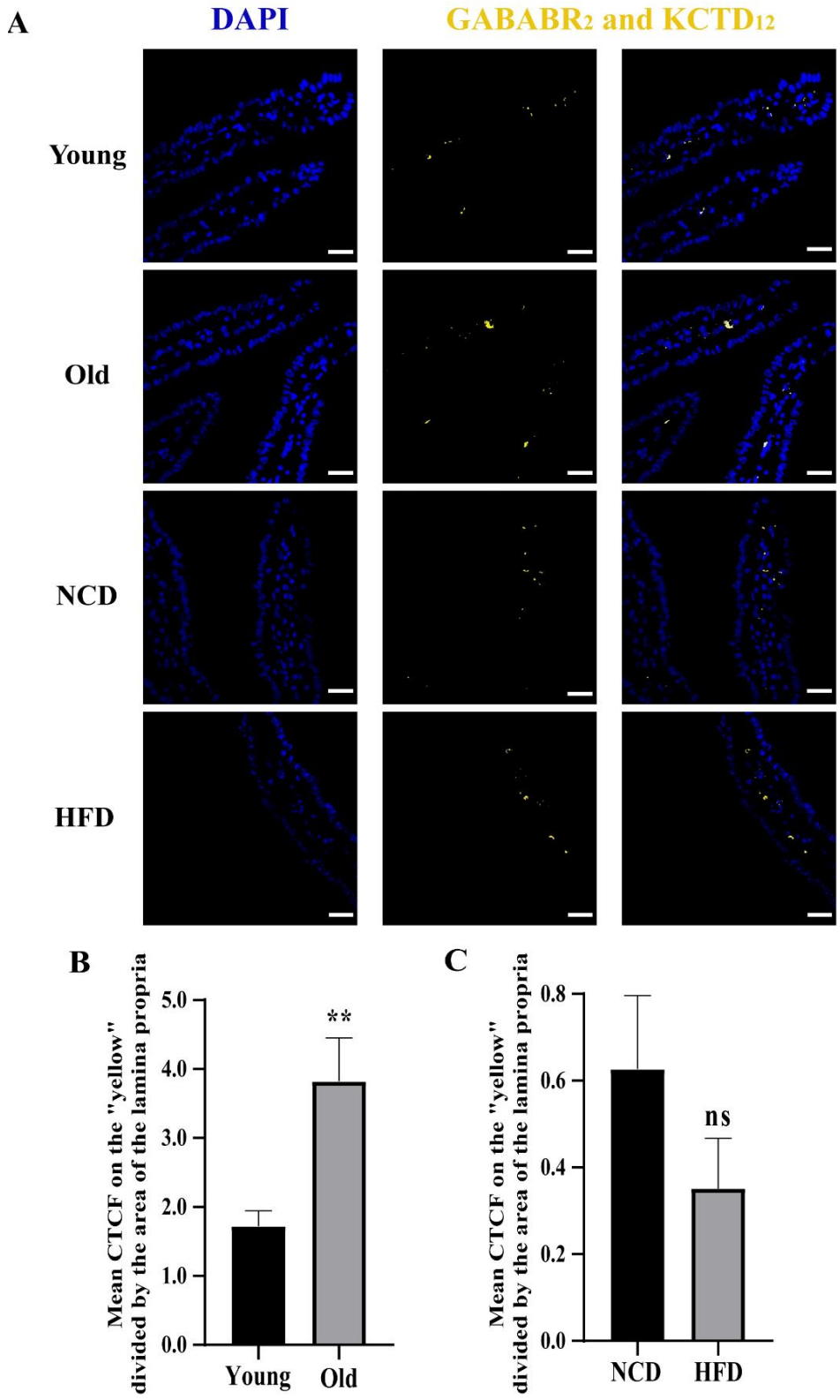

Figure 3.5: **$GABA_BR_2$ colocalized with $KCTD_{12}$ on proximal small intestinal sections from C57BL/6J male mice**. (**A**) PLA analysis (40x objective lens). PLA was performed with anti-$GABA_BR_2$ and anti-$KCTD_{12}$ primary antibodies, and their colocalization was detected by the presence of "yellow" bright spots. Cell nuclei were stained with DAPI ("blue"). **Scale bars**: 25 µm. (**B**-**C**) Quantification of the expression of $GABA_BR_2$ colocalized with $KCTD_{12}$ in young (4 months old) or old (20 months old) mice (**B**) or in NCD and HFD (prediabetes) mice (**C**) by CTCF normalized to the area of the lamina propria. All data are expressed as mean ± SEM and were obtained from (**B**) 177 villi analysed in n = 3 young (93 villi) and n = 2 old mice (84 villi), and from (**C**) 35 villi in n = 3 NCD (17 villi) and n = 4 HFD mice (18 villi). Statistical analyses were performed by unpaired t-test with Welch's correction. ns: not significant, $**p \leq 0.01$.

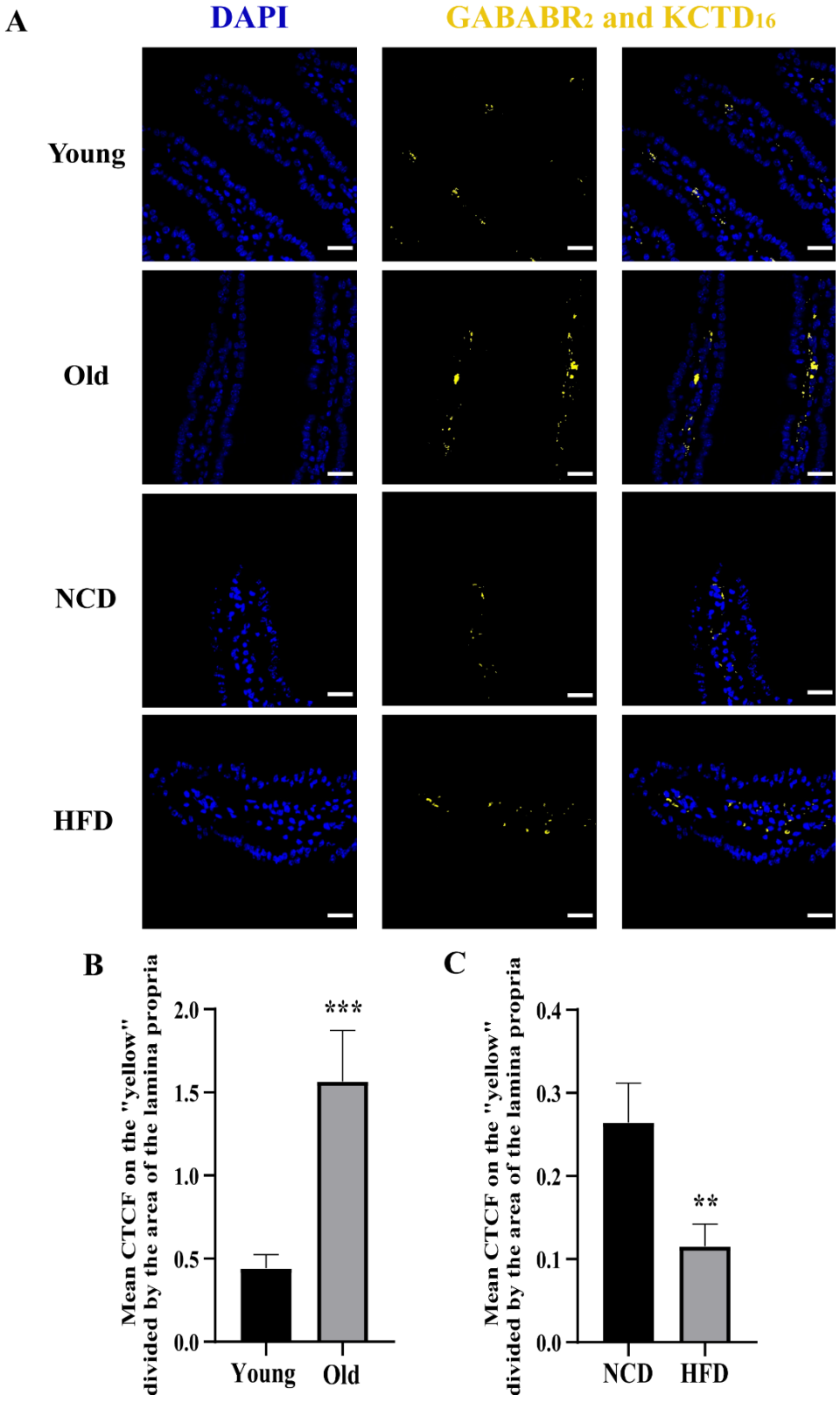

Figure 3.6: **$GABA_BR_2$ colocalized with $KCTD_{16}$ on proximal small intestinal sections from C57BL/6J male mice**. (**A**) PLA analysis (40x objective lens). PLA was performed with anti-$GABA_BR_2$ and anti-$KCTD_{16}$ primary antibodies, and their colocalization was detected by the presence of "yellow" bright spots. Cell nuclei were stained with DAPI ("blue"). **Scale bars**: 25 µm. (**B-C**) Quantification of the expression of $GABA_BR_2$ colocalized with $KCTD_{16}$ in young (4 months old) or old (20 months old) mice (**B**) or in NCD and HFD (prediabetes) mice (**C**) by CTCF normalized to the area of the lamina propria. All data are expressed as mean ± SEM and were obtained from (**B**) 182 villi analysed in n = 3 young (114 villi) and n = 2 old mice (68 villi), and from (**C**) 51 villi in n = 3 NCD (29 villi) and n = 4 HFD mice (22 villi). Statistical analyses were performed by unpaired t-test with Welch's correction. $^{**}p \leq 0.01$, $^{***}p \leq 0.001$.

3.4. GFAP positive cells not colocalized with KCTD proteins and their localization in proximal small intestinal sections

To analyse the impact of ageing or prediabetes on the number of glial cells present in the proximal small intestine, we quantified the differences in the expression of $GFAP^+/KCTD^-$ cells after IF staining [Figure 3.7 (A)], because $GABA_BR_2$ is expressed in almost all neurons and glial cells of the CNS, the latter being easily identified by GFAP expression.

It is important to note that a positive result was considered if 1) the ROI was only found on the "red" channel and had a Pearson and Li's correlation coefficient that were both negative (Table 2.1), or if 2) the normalized CTCF on the "green" channel was negative.

When we took into consideration young and old mice, we could observe an age-related increase in the expression of $GFAP^+/KCTD_{12}^-$ [old: 1.505 ± 0.568; young: 0.371 ± 0.098 (3.058-fold) – Figure 3.7 (C)] and $GFAP^+/KCTD_{16}^-$ cells [old: 1.419 ± 0.448; young: 0.423 ± 0.096 (2.353-fold, $p \leq 0.05$) – Figure 3.7 (D)]. The expression of $GFAP^+/KCTD_8^-$ cells was not determined due to shortage of anti-$KCTD_8$ primary antibody, but we expect the results to be quantitatively similar.

Furthermore, HFD also seemed to induce an increase in those expressions, except for $KCTD_{12}^-$ [$GFAP^+/KCTD_8^-$: 0.074 ± 0.034 for NCD, 0.395 ± 0.151 for HFD mice (4.316-fold, $p \leq 0.05$ – Figure 3.7 (B)); $GFAP^+/KCTD_{12}^-$: 0.200 ± 0.075 for NCD, 0.174 ± 0.053 for HFD mice (- 0.130-fold – Figure 3.7 (C)); $GFAP^+/KCTD_{16}^-$: 0.115 ± 0.025 for NCD, 1.406 ± 0.327 for HFD mice (11.26-fold, $p \leq 0.0001$ – Figure 3.7 (D))].

Since enteric glia is a key player in the modulation of CNS inflammation triggered by neuropathy, one of the most common complications associated with an increase in blood glucose levels, and overall similar conclusions are seen in old or HFD mice, we can assume that an inflammatory response is occurring in the proximal small intestine of these mice.

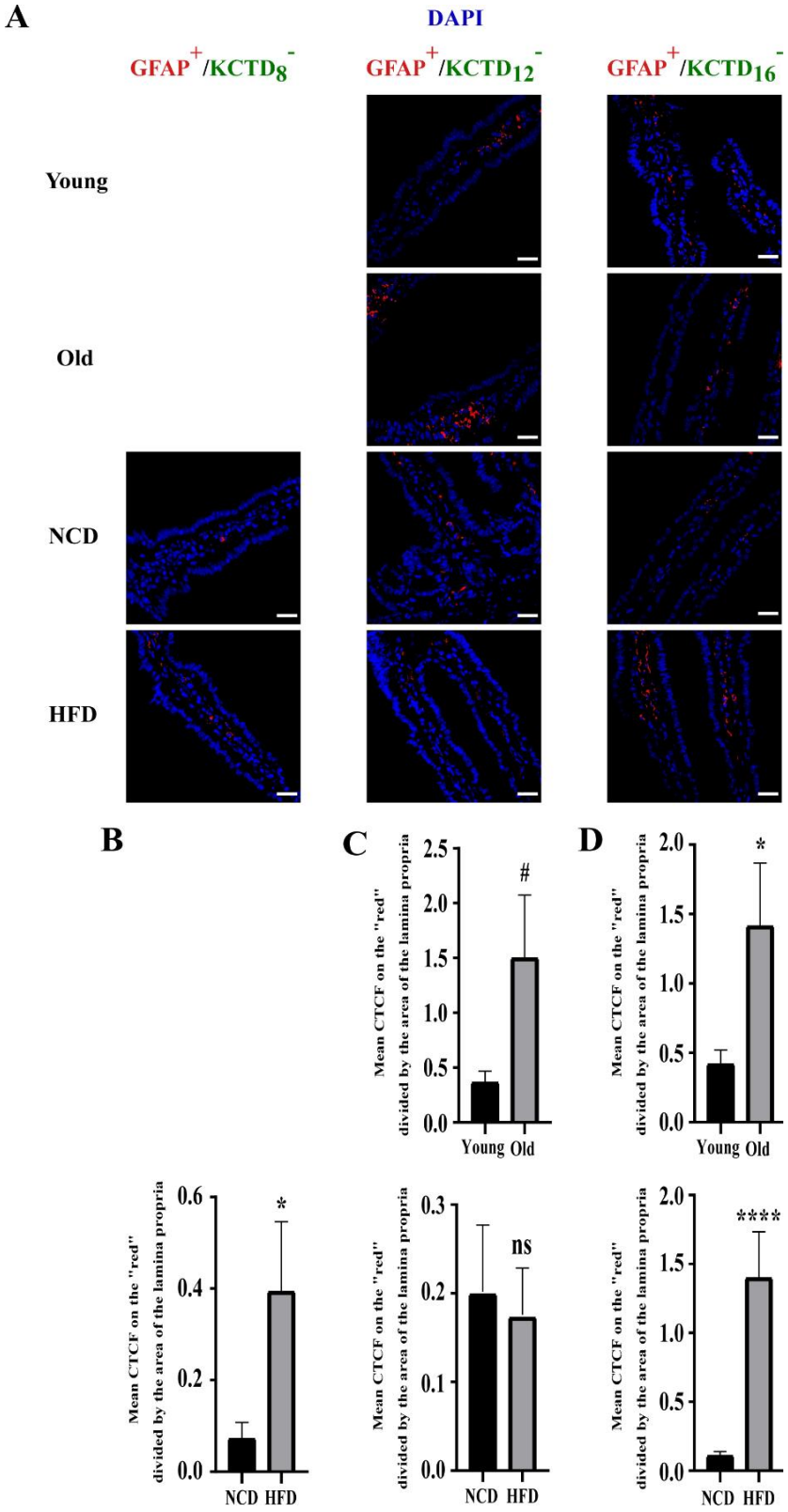

Figure 3.7: **GFAP$^+$/KCTD$^-$ cells on proximal small intestinal sections from C57BL/6J male mice**. (**A**) IF analysis (40x objective lens). GFAP expression is indicated by "red" fluorescence. Cell nuclei were stained with DAPI ("blue"). **Scale bars**: 25 µm. (**B-D**) Quantification of the expression of GFAP$^+$/KCTD$_8^-$ (**B**), GFAP$^+$/KCTD$_{12}^-$ (**C**) or GFAP$^+$/KCTD$_{16}^-$ cells (**D**) in C57BL/6J mice by CTCF normalized to the area of the lamina propria. Data were obtained from (**B**) 48 villi in n = 3 NCD (26 villi) and n = 4 HFD mice (prediabetes – 22 villi), (**C**) 56 villi in n = 3 young (31 villi) and n = 2 old mice (25 villi) and 54 villi in n = 3 NCD (29 villi) and n = 4 HFD mice (25 villi), and from (**D**) 57 villi in n = 3 young (30 villi) and n = 2 old mice (27 villi) and 58 villi in n = 3 NCD (33 villi) and n = 4 HFD mice (25 villi). All data are expressed as mean ± SEM. Statistical analyses were performed by unpaired t-test with Welch's correction. ns: not significant, #$p \leq 0.1$, *$p \leq 0.05$, ****$p \leq 0.0001$.

3.5. Determination of the localization of KCTD proteins not colocalized with enteric glia in the proximal small intestine

Although $KCTD_8$, $KCTD_{12}$ and $KCTD_{16}$ have been shown to form functional oligomers with $GABA_BR_2$ in neurons, resulting in the modulation of important signalling pathways, their importance in the proximal small intestine has not been elucidated, given that most studies have focused on their role in the brain (although $KCTD_{12}$ has been shown to exist in very small levels in the intestine[71]).

To clarify this, we quantified the differences in the expression of $GFAP^-/KCTD^+$ cells after IF staining with a specific primary antibody against each protein [Figure 3.8 (A)]. In other words, we will quantify GABAergic cells that are not glia, and would otherwise be expected to be GABAergic neurons or neuroendocrine cells.

In this case, a positive result was considered if 1) the ROI was only found on the "green" channel and had a Pearson and Li's correlation coefficient that were both negative (Table 2.1), or if 2) the normalized CTCF on the "red" channel was negative.

Taking into account the results obtained for young and old mice, it was possible to see that, even though the expression of $GFAP^-/KCTD_{12}^+$ cells showed an increasing trend [old: 0.419 ± 0.118; young: 0.163 ± 0.071 (1.573-fold) – Figure 3.8 (C)], $GFAP^-/KCTD_{16}^+$ cell expression was statistically decreased due to increased age [old: 0.024 ± 0.010; young: 0.080 ± 0.016 (- 0.701-fold, $p \leq 0.01$) – Figure 3.8 (D)]. The expression of $GFAP^-/KCTD_8^+$ cells was not determined due to shortage of anti-$KCTD_8$ primary antibody.

Similarly, HFD also seemed to display an ambiguity when it comes to these expressions, although the statistically significant increase of $GFAP^-/KCTD_{12}^+$ cell expression could be indicative of an increase in $KCTD_{12}$-expressing neural cells within prediabetic mouse models [$GFAP^-/KCTD_8^+$: 0.016 ± 0.005 for NCD, 0.012 ± 0.007 for HFD mice (- 0.240-fold – Figure 3.8 (B)); $GFAP^-/KCTD_{12}^+$: 0.0007 ± 0.0005 for NCD, 0.033 ± 0.009 for HFD mice (49.73-fold, $p \leq 0.001$ – Figure 3.8 (C)); $GFAP^-/KCTD_{16}^+$: 0.006 ± 0.003 for NCD, 0.051 ± 0.030 for HFD mice (7.583-fold – Figure 3.8 (D))].

We have shown that $GFAP^-/KCTD^+$ cells are present in the lamina propria, but in several villi, these also appear on the basal side of the epithelial layer of the mucosa. $GABA_BR_2^-/KCTD^+$ cells were also observed on the basal side in IF double-staining assay of $GABA_BR_2$ and $KCTD_8$ performed on NCD and HFD mice (Figure 3.9), and in previous optimization processes. These KCTD proteins are most likely present in serotonergic enterochromaffin cells as well since serotonin is also a neurotransmitter.

The total amount of KCTD positive cells without colocalization with $GABA_BR_2$ or GFAP on the basal side of the epithelial layer of the mucosa is expressed in Table 3.1:

Table 3.1: **Total number of $GABA_BR_2^-/KCTD^+$ and $GFAP^-/KCTD^+$ cells on the basal side of the epithelial layer of the mucosa in intestinal villi**. Total number of $GFAP^-/KCTD_8^+$ cells in young and old C57BL/6J male mice were not determined due to shortage of anti-$KCTD_8$ primary antibody. $GABA_BR_2^-/KCTD^+$ cells were not counted is most mice due to the nature of the PLA, but they were observed in the IF double-staining assay performed on NCD and HFD (prediabetes) mice (done only for $KCTD_8$) and in previous optimization studies.

Mouse model	$KCTD_8^+$	$KCTD_{12}^+$	$KCTD_{16}^+$
Young	----------	18 $GFAP^-$	29 $GFAP^-$
Old	----------	15 $GFAP^-$	24 $GFAP^-$
NCD	3 $GABABR_2^-$ 12 $GFAP^-$	11 $GFAP^-$	7 $GFAP^-$
HFD	9 $GABABR_2^-$ 19 $GFAP^-$	23 $GFAP^-$	19 $GFAP^-$

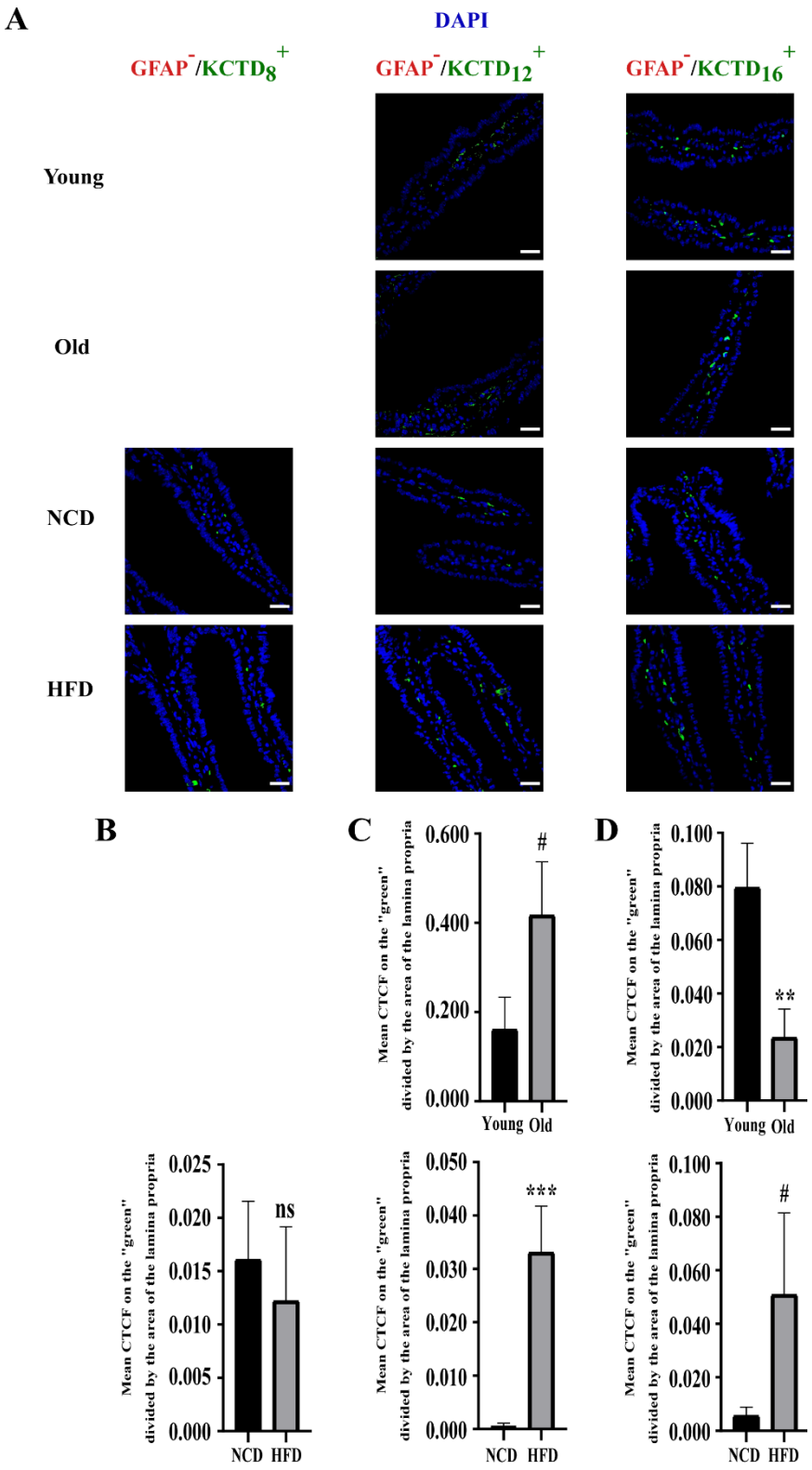

Figure 3.8: **GFAP$^-$/KCTD$^+$ cells on proximal small intestinal sections from C57BL/6J male mice**. (**A**) IF analysis (40x objective lens). KCTD protein expression is indicated by "green" fluorescence. Cell nuclei were stained with DAPI ("blue"). **Scale bars**: 25 µm. (**B-D**) Quantification of the expression of GFAP$^-$/KCTD$_8^+$ (**B**), GFAP$^-$/KCTD$_{12}^+$ (**C**) or GFAP$^-$/KCTD$_{16}^+$ cells (**D**) in C57BL/6J mice by CTCF normalized to the area of the lamina propria. Data were obtained from (**B**) 48 villi in n = 3 NCD (26 villi) and n = 4 HFD mice (prediabetes – 22 villi)], (**C**) 56 villi in n = 3 young (31 villi) and n = 2 old mice (25 villi) and 54 villi in n = 3 NCD (29 villi) and n = 4 HFD mice (25 villi), and from (**D**) 57 villi in n = 3 young (30 villi) and n = 2 old mice (27 villi)] and 58 villi in n = 3 NCD (33 villi) and n = 4 HFD mice (25 villi). All data are expressed as mean ± SEM. Statistical analyses were performed by unpaired t-test with Welch's correction. ns: not significant, #$p \leq 0.1$, **$p \leq 0.01$, ***$p \leq 0.001$.

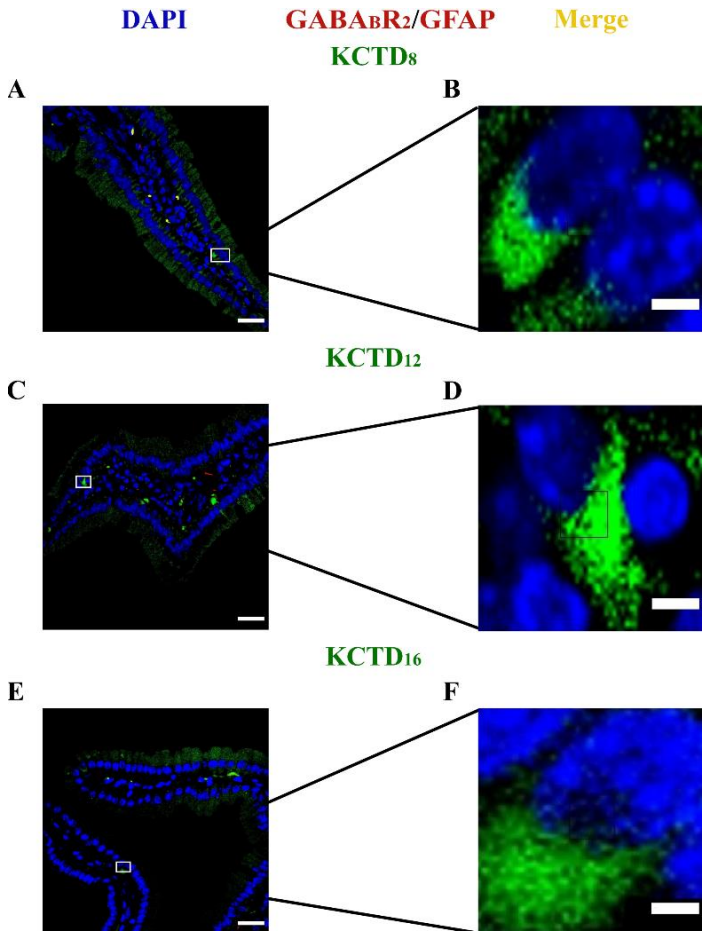

Figure 3.9: **KCTD proteins and their presence on the basal side of the epithelial layer of the mucosa in intestinal villi**. In the proximal small intestine, $KCTD_8$ (**A**), $KCTD_{12}$ (**C**) and $KCTD_{16}$ (**E**) can be positioned on the basal side of the epithelial layer of the mucosa without any colocalization whatsoever with $GABA_BR_2$ or GFAP. $GABA_BR_2$ or GFAP expression is indicated by "red" fluorescence, while "green" fluorescence corresponds to KCTD. **B**, **D** and **F** denote a 5x magnified projection of the isolated KCTD proteins boxed in **A**, **C** and **E** respectively. **Scall bars**: 25 µm (**A**), 15 µm (**B**).

3.6. Differences in localization and spatial relationships between KCTD proteins and enteric glial cells

To investigate the differences in localization and spatial relationships relative to KCTDs and enteric glial cells, an IF assay was performed, and the expression of GFAP colocalized with each KCTD protein was determined. The ROIs that had a Pearson and Li's correlation coefficient bigger or equal than those indicated on Table 2.1 were considered as positive results.

Considering the expression of GFAP and $KCTD_8$ positive cells, we were able to determine that HFD induced a decreasing trend on that expression [NCD: 0.166 ± 0.119, HFD: 0.017 ± 0.009 when we consider the normalized mean CTCF obtained on the "red" channel (- 0.898-fold); NCD: 0.219 ± 0.158 (9.74% of total ROI), HFD: 0.015 ± 0.009 (7.50%) for the normalized mean CTCF obtained on the "green" channel (- 0.933-fold) – Figure 3.10]. This expression was not determined in young or old mice due to shortage of anti-$KCTD_8$ primary antibody.

In the case of the expression of GFAP colocalized with $KCTD_{12}$, we observed an age-related statistically significant increase on that expression [old: 0.998 ± 0.296, young: 0.189 ± 0.059 when we consider the normalized mean CTCF obtained on the "red" channel (4.280-fold, $p \leq 0.05$); old: 0.981 ± 0.280 (11.5% of total ROI), young: 0.141 ± 0.049 (9.94%) for the normalized mean CTCF obtained on the "green" channel (5.942-fold, $p \leq 0.01$) – Figure 3.11 (A) and 3.11 (B)]. HFD induced a decreasing trend [NCD: 0.102 ± 0.046, HFD: 0.037 ± 0.013 when we consider the normalized mean CTCF obtained

on the "red" channel (- 0.640-fold); NCD: 0.041 ± 0.020 (15.0% of total ROI), HFD: 0.063 ± 0.037 (9.77%) for the normalized mean CTCF obtained on the "green" channel (0.523-fold) – Figure 3.11 (A) and 3.11 (C)].

These conclusions were also alike when we took into consideration the effect of ageing on the expression of GFAP colocalized with $KCTD_{16}$, as it induced a statistically significant increase [old: 0.807 ± 0.169, young: 0.037 ± 0.021 when we consider the normalized mean CTCF obtained on the "red" channel (20.87-fold, $p \leq 0.001$); old: 0.730 ± 0.157 (28.8% of total ROI), young: 0.043 ± 0.022 (6.18%) for the normalized mean CTCF obtained on the "green" channel (15.83-fold, $p \leq 0.001$) – Figure 3.12 (A) and 3.12 (B)].

However, and unlike what we saw for $KCTD_8$ and $KCTD_{12}$, HFD induced a statistically significant decrease on the expression of GFAP and $KCTD_{16}$ positive cells [NCD: 0.083 ± 0.024, HFD: 0.006 ± 0.003 when we consider the normalized mean CTCF obtained on the "red" channel (- 0.923-fold, $p \leq 0.01$); NCD: 0.022 ± 0.006 (15.5% of total ROI), HFD: 0.009 ± 0.005 (2.75%) for the normalized mean CTCF obtained on the "green" channel (- 0.604-fold) – Figure 3.12 (A) and 3.12 (C)].

Overall, these observations allowed us to infer that the decreased number of $KCTD_{16}$-expressing enteric glia in prediabetic mouse models may be involved in disrupted $GABA_BR$ signalling within enteric glia in prediabetes independent of age.

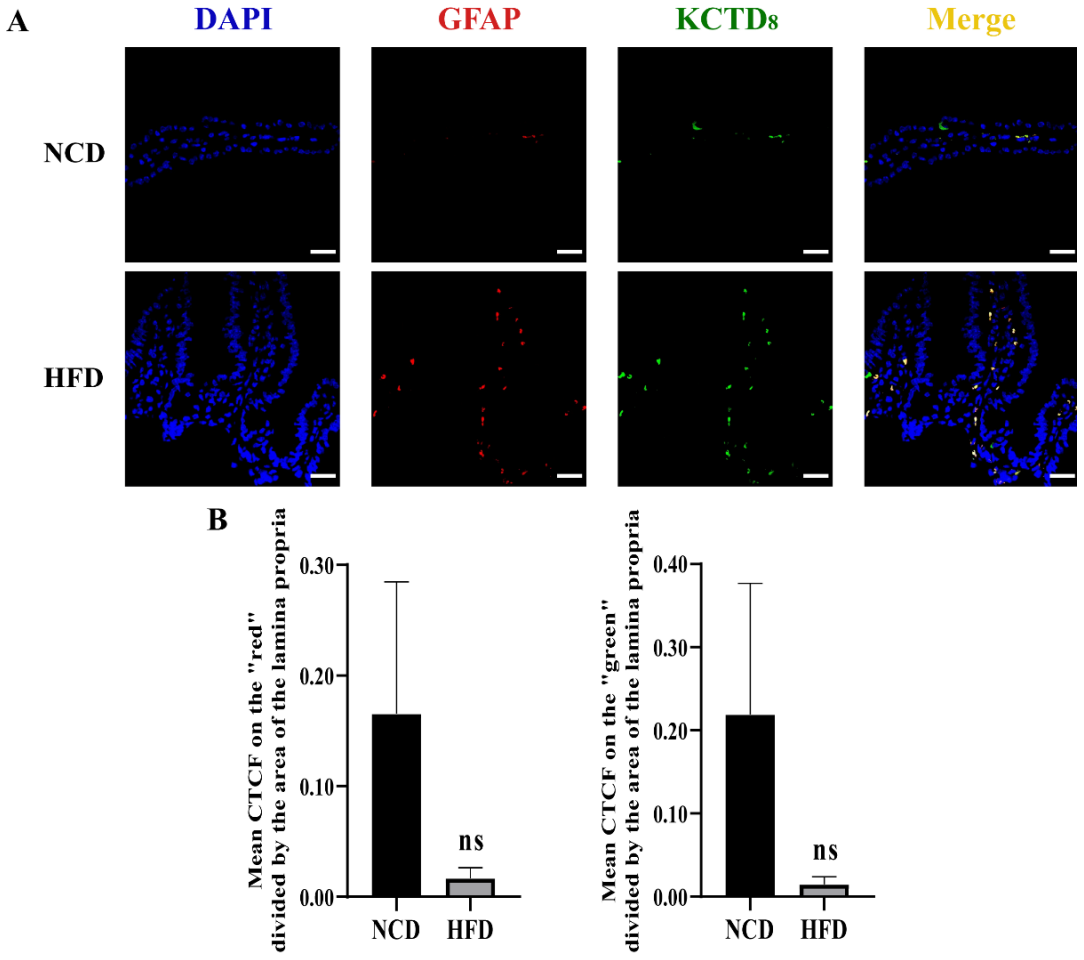

Figure 3.10: **GFAP colocalized with $KCTD_8$ on proximal small intestinal sections from NCD and HFD (prediabetes) C57BL/6J male mice**. (**A**) IF analysis (40x objective lens). Cell nuclei were stained with DAPI ("blue"). GFAP expression is indicated by "red" fluorescence, while "green" fluorescence corresponds to $KCTD_8$. Possible GFAP and $KCTD_8$ positive cells are indicated as "yellow" fluorescence. **Scale bars**: 25 µm. (**B**) Quantification of the expression of GFAP colocalized with $KCTD_8$ by CTCF normalized to the area of the lamina propria. All data are expressed as mean ± SEM and were obtained from 48 villi in n = 3 NCD (26 villi) and n = 4 HFD mice (22 villi). Statistical analyses were performed by unpaired t-test with Welch's correction. ns: not significant.

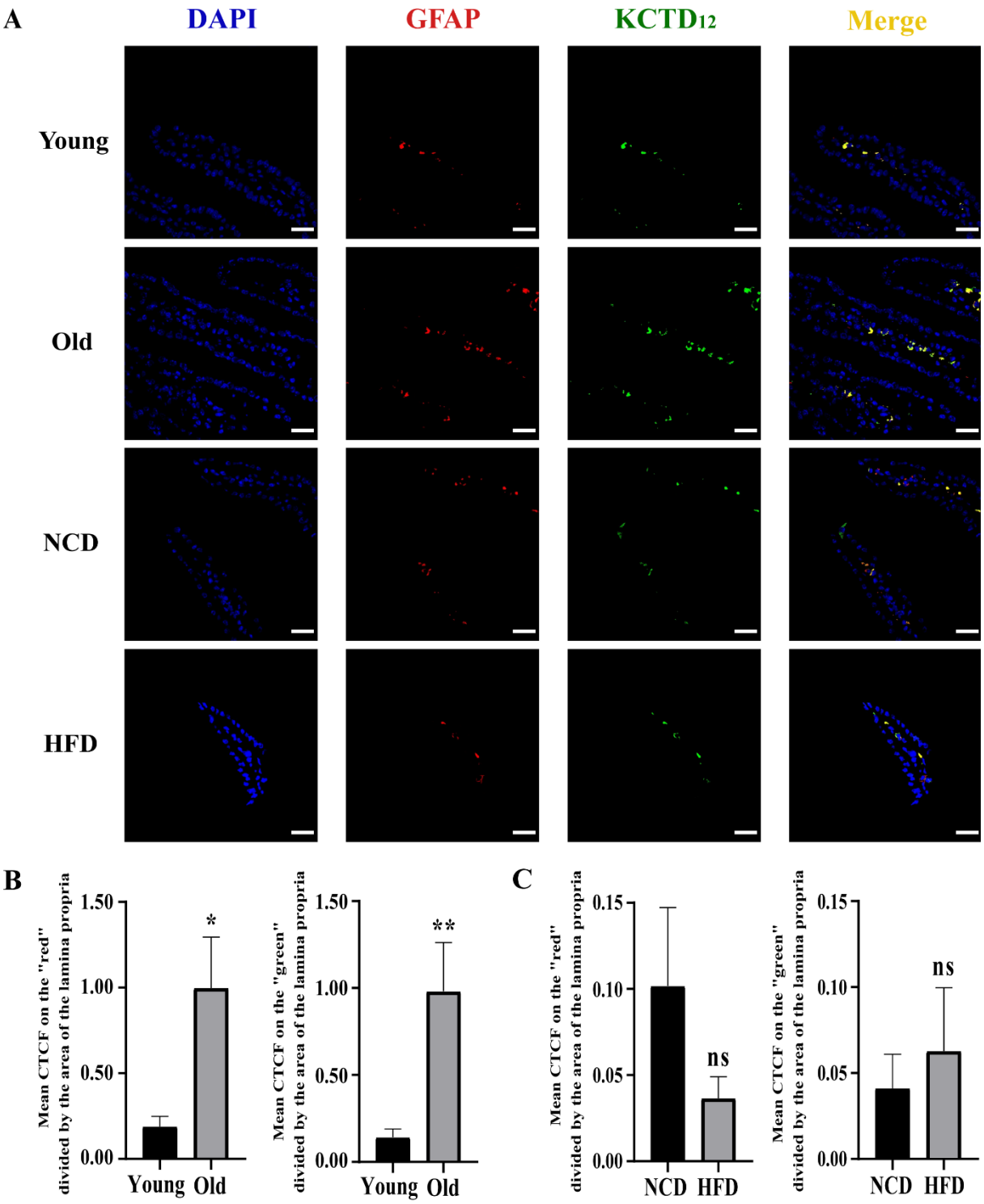

Figure 3.11: **GFAP colocalized with KCTD$_{12}$ on proximal small intestinal sections from C57BL/6J male mice**. (**A**) IF analysis (40x objective lens). Cell nuclei were stained with DAPI ("blue"). GFAP expression is indicated by "red" fluorescence, while "green" fluorescence corresponds to KCTD$_{12}$. Possible GFAP and KCTD$_{12}$ positive cells are indicated as "yellow" fluorescence. **Scale bars**: 25 µm. (**B**-**C**) Quantification of the expression of GFAP colocalized with KCTD$_{12}$ in young (4 months old) or old (20 months old) mice (**B**) or in NCD and HFD (prediabetes) mice (**C**) by CTCF normalized to the area of the lamina propria. All data are expressed as mean ± SEM and were obtained from (**B**) 56 villi in n = 3 young (31 villi) and n = 2 old mice (25 villi) and from (**C**) 54 villi in n = 3 NCD (29 villi) and n = 4 HFD mice (25 villi). Statistical analyses were performed by unpaired t-test with Welch's correction. ns: not significant, *$p \leq 0.05$, **$p \leq 0.01$.

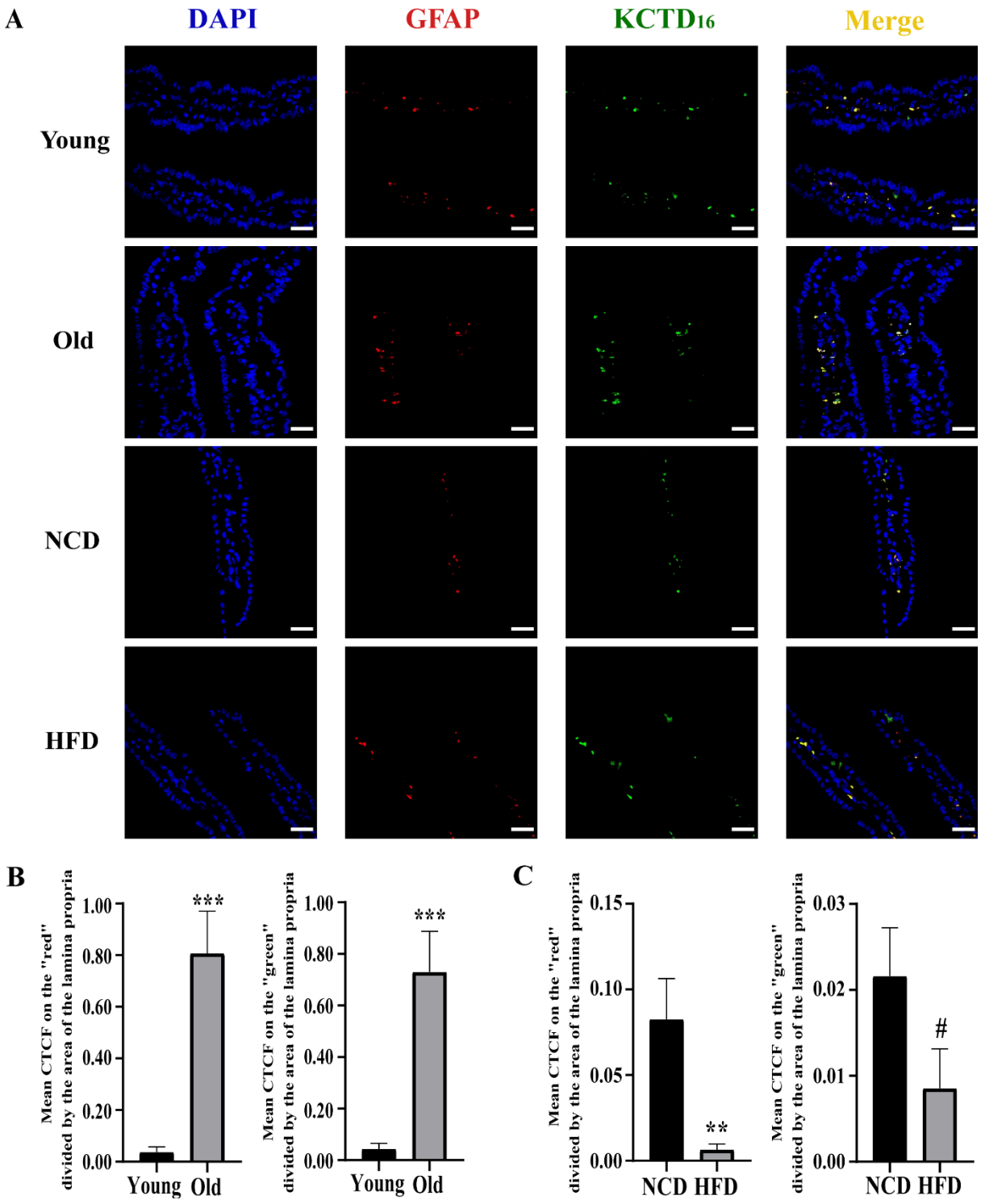

Figure 3.12: **GFAP colocalized with KCTD$_{16}$ on proximal small intestinal sections from C57BL/6J male mice**. (**A**) IF analysis (40x objective lens). Cell nuclei were stained with DAPI. GFAP expression is indicated by "red" fluorescence, while "green" fluorescence corresponds to KCTD$_{16}$. Possible GFAP and KCTD$_{16}$ positive cells are indicated as "yellow" fluorescence. **Scale bars**: 25 µm. (**B**-**C**) Quantification of the expression of GFAP colocalized with KCTD$_{16}$ in young (4 months old) or old (20 months old) mice (**B**) or in NCD and HFD (prediabetes) mice (**C**) by CTCF normalized to the area of the lamina propria. All data are expressed as mean ± SEM and were obtained from (**B**) 57 villi in n = 3 young (30 villi) and n = 2 old mice (27 villi) and from (**C**) 58 villi in n = 3 NCD (33 villi) and 4 HFD mice (25 villi). Statistical analyses were performed by unpaired t-test with Welch's correction. #$p \leq 0.1$, **$p \leq 0.01$, ***$p \leq 0.001$.

4. Discussion

The prevalence of DM increases with age, the highest being in individuals older than 65 years old. This estimated prevalence corresponded to 134 million in 2019 (19.3% of the world population older than 65 years old at the time) and is expected to rise to 276 million (19.6%) by 2045, pinpointing age as one of the main risk factors for the development of this disease. This classifies DM as a serious health hazard that needs to be dealt with to reduce the need of continued medical care and the stress and healthcare costs associated with it, and to increase the quality of life and diminish its high early mortality rate[2,23].

T2DM, which accounts for around 90% of all DM cases worldwide, arises from 1) an impairment in the ability of muscle, fat, and liver cells to respond to insulin (insulin resistance), and from 2) the inability of the β-cells of the pancreatic islets of Langerhans to increase insulin secretion after an upsurge in blood glucose levels. These increased levels will generate an abnormal accumulation of glucose in the bloodstream over a prolonged period of time (hyperglycaemia)[9,96].

Before the development of full-blown T2DM (prediabetes), no hyperglycaemia is observed, but individuals present themselves with impaired fasting glucose and impaired glucose tolerance, phenomena that can last many years, and where early prevention and remission could be achieved[75,97].

Thus, our first objective was to determine if our C57BL/6J male mouse models of ageing and HFD-induced prediabetes had impaired fasting glucose or glucose intolerance, by measuring fasting blood glucose levels and subjecting them to an IPGTT (done only in NCD and HFD-fed mouse cohorts). Both old and HFD mice had an increase in their body weight [Figure 3.1 (A) and Figure 3.2 (A) respectively], when compared to young and NCD mice respectively. HFD mice presented glucose intolerance and high blood glucose levels even after 120 minutes of intraperitoneal glucose injection [Figure 3.2 (B) and 3.2 (C)], while no difference was observed in the fasting blood glucose levels of old mice (20 months old), when compared to the young ones [4 months old – Figure 3.1 (B)]. Unfortunately, we did not have the opportunity of performing an IPGTT on young and old mice, which were obtained during the early stages of the coronavirus pandemic that coincided with the closure of our animal facility.

Although we cannot say for sure that old mice had no glucose intolerance, we confirmed that 1) the HFD-induced prediabetic model represented prediabetes with impaired fasting glucose and glucose intolerance, and that 2) the old mouse models were not prediabetic with respect to fasting glycaemia.

In normal conditions, the gut contains endocrine cells that communicate with enteric glia and neurons using both hormones and neurotransmitters in response to ingested nutrients and other molecules. Therefore, correct entero-neuroendocrine communication is essential for the regulation of glucose homeostasis[48]. One of the most prominent inhibitory neurotransmitters present in the developmentally mature mammalian CNS is GABA, a neurotransmitter that binds to specific transmembrane receptors in the plasma membrane of both pre- and postsynaptic neuronal processes, such as $GABA_BR$, and leads to a regulation of nerve excitability and a stabilization of resting membrane potential[61]. $GABA_BR_2$ transduce signalling via intracellular KCTD auxiliary subunits, namely $KCTD_8$, $KCTD_{12}$ and $KCTD_{16}$, that provide diversity of intracellular responses to the extracellular binding of the neurotransmitter GABA to the $GABA_BRs$[73].

Therefore, our second objective was to study $GABA_BR$ distribution and their auxiliary KCTD subunits in the proximal small intestine of prediabetic mice or in mice with an increased age. We chose to do these assays on the proximal small intestine since it is one of the possible major culprits in the aetiology of T2DM, as evidenced by the remission of this pathological condition within days of bariatric surgery that involved a bypass of this gut region, such as RYGB[98]. PLA [Figure 3.4 (A), Figure 3.5 (A) and Figure 3.6 (A)] and IF analyses [Figure 3.4 (B)] showed an age-related statistically significant increase in the expression of $GABA_BR_2$ colocalized with either $KCTD_8$ [Figure 3.4 (C)], $KCTD_{12}$ [Figure 3.5 (B)] or $KCTD_{16}$ [Figure 3.6 (B)]. More importantly, HFD-induced prediabetes had the

opposite effect on those expressions [Figure 3.4 (D) for $KCTD_8$, Figure 3.5 (C) for $KCTD_{12}$ – decreasing trend – and Figure 3.6 (C) for $KCTD_{16}$].

A previous study done by Zheng *et al*. has shown that the activation of $GABA_BR$ (heterodimer containing $GABA_BR_1$ and $GABA_BR_2$ subunits) causes a dissociation between the heterodimer $G_{\beta\gamma}$ and G_α. $G_{\beta\gamma}$ remains attached to the membrane by its lipid anchor, resulting in the activation of the G protein-coupled inwardly-rectifying potassium channel (GIRK) while KCTD is at a relatively low concentration, and an outflow of K^+ (depolarization). When KCTD increases in concentration, it will also bind to the GIRK-bound $G_{\beta\gamma}$ subunit, but since GIRK has a higher affinity and cooperativity to KCTD, the $G_{\beta\gamma}$ heterodimer will be stripped from GIRK and the channel will be deactivated (hyperpolarization)[99].

Following GTP hydrolysis by adenylyl cyclase, GDP-bound G_α will bind once more to the free $G_{\beta\gamma}$ heterodimer, sequestering the GIRK channel from KCTD and restoring the system for another signalling cycle[99]. Once detached from GIRK, KCTD will bind to the C-terminus of $GABA_BR_2$ as a tetramer, stabilizing G proteins at the receptor and controlling the time course of the G protein-mediated receptor response[100].

It is important to note that the study done by Zheng *et al*. only reports to $KCTD_{12}$. This is due to previous results that show a fast and pronounced current desensitization for this protein, caused by the H_1 homology domain present in it (essential T/NFLEQ motif), and currents with little desensitization for $KCTD_8$ and $KCTD_{16}$ due to the presence of an antagonistic H_2 homology domain that inhibits desensitization induced by H_1[68]. Despite this difference, our results allowed us to infer that the regulation of $GABA_BR$ signalling by KCTD proteins is affected in prediabetic mice, more evidently in the slow-desensitizing proteins, and could potentially be an interesting target for future therapies.

T2DM is characterized, not just by insulin resistance and loss of pancreatic β-cell function as previously mentioned, but also by islet autoreactivity, a factor that can be generally measured by the presence of auto-antibodies directed towards β-cells, such as GAD_{65}[13]. GAD_{65} is usually expressed in the nerve terminals and in the insulin-producing β-cells of the pancreas (only isoform present in humans), in varying ratios depending upon the species[101,102]. This enzyme represents an important biomarker and immunotherapy target for the risk and progression of DM, given that immunoreactivity to this specific DM-associated self-antigen has been reported in prediabetic subjects[102,103].

These specific auto-antigens are expressed in pancreatic β-cells and in cells that compose the surrounding nervous system, which include the peri-islet Schwann cells that are identified by GFAP expression[104]. GFAP is also expressed in enteric glia of the ENS, more prominently those contained within the myenteric plexus, with a higher level than in astrocytes and Schwann cells, probably due to cues from the gut microenvironment[105]. These non-myelinating peripheral glial cells that reside within the walls of the intestinal tract interact with various non-neuronal cell types, such as enterocytes and immune cells, and are important for maintaining the GI functions and influencing gut physiology and pathophysiology, which justifies GFAP labelling in our study[106].

Neuroinflammation is a fundamental innate and adaptive immune reaction in both the CNS and the PNS, in response to either pathogens or host-derived signals of cellular damage. Glia, the resident immune cells of the nervous system, deal directly with foreign molecules and tissue damage by a gradual activation process that includes morphological changes and the secretion of molecular signals. This process can trigger an acute inflammatory response that aims to repair the damaged area[107]. If the stimuli that led to this inflammatory response persist in time, a chronic inflammatory condition develops, causing persistent activation of glia, and inducing complex interactions and feedback loops between glial and neuronal cells that can lead to neuronal damage[108].

Hence, our third and final objective was to quantify the differences in localization and spatial relationships of the $GABA_BR_2$ auxiliary KCTD subunits relative to enteric glial cells. First, we characterized the differences in the expression of $GFAP^+/KCTD^-$ cells by IF staining [Figure 3.7 (A)] in the proximal small intestine of prediabetic mice or in mice with an increased age. We found an increase

in the expression of $GFAP^+/KCTD^-$ cells with increased age [Figure 3.7 (C) and 3.7 (D) (increasing trend)] and in most HFD-induced prediabetic conditions [Figure 3.7 (B) and 3.7 (D)]. This is in agreement with previous reports that suggest that ageing is characterized by a chronic, low-grade inflammatory process, termed "inflammaging", whose main causes include the accumulation of cell senescence, gut dysbiosis and immune-senescence[109]. This process can be beneficial for the individual, given that most centenaries present themselves with high plasma levels of pro-inflammatory cytokines, such as IL-6 and IL-8, as well as decreased antioxidant defenses, but they are also able to avoid or delay the onset of chronic age-related pathologies, such as T2DM, suggesting that "inflammaging" state could be compatible with health and longevity. This "protection" will only occur if anti-inflammatory responses are able to counteract those inflammatory processes[110].

Nevertheless, the observed increased expression of $GFAP^+/KCTD^-$ cells in all old mice and most prediabetic mouse models demonstrates a recruitment of activated enteric glia to the proximal small intestine, hinting at a normal immune response. The extent of this process and if it is inducing beneficial (acute) or deleterious (chronic) effects is yet to be evaluated.

When comparing the expression of $GFAP^-/KCTD^+$ cells by IF studies [Figure 3.8 (A)], the results obtained were more ambiguous. $GFAP^-/KCTD_8^+$ cell expression, which was only measured in NCD and HFD mice, showed no distinguishable difference [Figure 3.8 (B)]. On the other hand, $GFAP^-/KCTD_{12}^+$ cells had a higher expression in HFD mice [Figure 3.8 (C)], while $GFAP^-/KCTD_{16}^+$ cell expression was decreased in old mice [Figure 3.8 (D)]. These $GFAP^-/KCTD^+$ cells, as well as $GABA_BR_2^-/KCTD^+$ cells, were observed in the lamina propria and on the basal side of the epithelial layer of the mucosa (Figure 3.9 and Table 3.1). This observation hints at a possible correlation between KCTD proteins and serotonergic cells, because 95% of the body's serotonin is synthetized, stored and released from enterochromaffin cells present in the intestinal mucosa, where it can play vital roles as a growth factor, a hormone, a paracrine factor, and a neurotransmitter[111,112,113].

Previous studies done by Metz *et al*. have shown that *KCTD12* is expressed in a wide array of organs, such as nervous system and liver (high levels), intestine, colon, kidney, heart and lung (low levels), while *KCTD8* and *KCTD16* were only expressed in the nervous system and eye[71]. While more studies need to be done to strengthen our observations, this is the first one that displays $KCTD_8^+$ or $KCTD_{16}^+$ cells being expressed in the lamina propria and on the basal side of the epithelial layer of the mucosa, albeit at low expression, without colocalization with $GABA_BR_2$ or GFAP. Since $KCTD_{12}$ alone was the only protein that had a statistically significant increase in prediabetes (Figure 3.8), we could infer that non-glial, but probably exclusively neural cells expressing $KCTD_{12}$, may be increased in our prediabetic mouse model independent of age.

To finalize the third objective, the differences in the expression of GFAP positive cells colocalized with each KCTD protein were determined through IF studies [Figure 3.10 (A), Figure 3.11 (A) and Figure 3.12 (A)]. Ageing generated a statistically significant increase in the expression of $GFAP^+/KCTD_{12}^+$ [Figure 3.11 (B)] and $GFAP^+/KCTD_{16}^+$ cells [Figure 3.12 (B)]. HFD-induced prediabetes provoked the opposite effect, albeit with significant decrease only observed for $KCTD_{16}$ [Figure 3.12 (C)].

Charles *et al*. were the first to demonstrate that $GABA_BR_2$ is expressed at the protein level in activated microglia and astrocytes of the rat CNS[114], the latter responding to the activation of the receptor, with delayed glial calcium transients induced by $GABA_BR_2$ activation occurring more prominently during a time of postnatal development when hippocampal networks are established[115]. In that sense, we may assume that elucidating the expression of KCTD proteins colocalized with GFAP indirectly exemplifies that they are associated with $GABA_BR_2$ present in enteric glia.

Since the results demonstrated throughout this objective are very similar to those obtained in our second objective, it is safe to assume that enteric glia is possibly involved in the dysfunction of $KCTD_{16}$-mediated regulation of $GABA_BR$ signalling within enteric glia in prediabetes independent of

age. Conversely, in old mice, expression of $GFAP^+/KCTD_{16}^+$ cells is increased, further supporting the idea that $KCTD_{16}$ could be used as a pharmacological target to study prediabetes prevention.

Even though interesting conclusions have been withdrawn, they are not as conclusive as they could have been, since one of the main limitations regarding this sort of analyses consists in the autofluorescence of tissue sections, which can produce confounding results (false positives) in immunohistochemical labelling. This autofluorescence can be stronger or equal to the intensity of that labelling, and may derive from several endogenous fluorophores, including collagen/elastin, fatty acids, flavins, lipofuscin, NAD(P)H, and/or vitamin A[116].

Despite all these, in this study, we noticed that the main source of autofluorescence corresponded to erythrocytes (Figure 3.3), more specifically the protoporphyrin contained in their heme group, that usually emits bright autofluorescence at 488 nanometres [spectra of fluorescein isothiocyanate (FITC)] and 555 nanometres [spectra of tetramethylrhodamine-isothiocyanate (TRITC)]. These wavelengths usually span with the emission and excitation spectra of many commonly used fluorescent reporters, such as antibodies[117,118].

Ideally, optimization could be achieved by performing an intravascular treatment with erythrocyte lysis solution before a routine perfusion with normal saline and formalin, combined with the Sudan Black B^{TM} treatment after antigen retrieval. This treatment has been shown to have very prominent results in regards to the improvement of the resolution of immunohistochemical labelling in liver and kidney sections[117].

4.1. Main conclusions

In this study, we analysed proximal small intestinal sections from C57BL/6J male mouse models of ageing and prediabetes.

We showed that all three non-glial $KCTD^+/GFAP^-$ cells studied are present in the lamina propria, with $KCTD_{12}^+$ substantially increased in HFD-induced prediabetic mice, and $KCTD_{16}^+$ decreased in old mice. On the basal side of the epithelial layer of the mucosa, non-$GABA_BR_2^+$ and non-glial $KCTD^+$ cells were also observed. Hence, we infer that $KCTD_{12}$ could be a potential biomarker of prediabetic changes in the gut independent of age, and further research should be done to clarify how HFD stimulates these changes, and if potential downstream signalling consequences affect glucose metabolism.

Finally, the colocalization of $GABA_BR_2$ membrane receptor and its auxiliary subunits $KCTD_8$ and $KCTD_{16}$ was decreased in the lamina propria of prediabetic mice. GFAP colocalization with $KCTD_{16}$ was also decreased in these prediabetic mouse models. This indicates that the decreased number of $KCTD_{16}$-expressing enteric glia is likely to be involved in disrupted $GABA_BR$ signalling within $GFAP^+$ enteric glia in prediabetes independent of age. Given the important role of enteric glia in enteric neuronal cell homeostasis, we should further investigate how these changes in $KCTD_{16}$ expression affect enteric glial function in prediabetes.

4.2. Future perspectives

These results will need to be replicated in a larger cohort of animals with 1) glucose intolerance determined in models of ageing, 2) the autofluorescence problems addressed, and with 3) other enteric cell types explored, such as serotonergic enterochromaffin cells. We will also need to clarify exactly how gut-disrupted expression of KCTDs is involved in the regulation of membrane potential and calcium signalling, in response to ingested nutrients, and if it affects glucose homeostasis in prediabetes.

Notwithstanding, these results have great potential to further investigate the possible underlying causes of T2DM and discover pharmacological targets in the prediabetic stage that could prevent disease progression and achieve remission.

5. References

1. Zhou, B., Lu, Y., Hajifathalian, K. & Bentham, J. Worldwide trends in diabetes since 1980: a pooled analysis of 751 population-based studies with 4.4 million participants. *Lancet* **387**, 1513–1530 (2016).
2. Federation, I. D. *IDF Diabetes Atlas, Ninth Edition*. (2019).
3. Barreto, M. *et al.* Prevalence, awareness, treatment and control of diabetes in Portugal: Results from the first National Health examination Survey (INSEF 2015). *Diabetes Res. Clin. Pract.* **140**, 271–278 (2018).
4. Mergenthaler, P., Lindauer, U., Dienel, G. A. & Meisel, A. Sugar for the brain: The role of glucose in physiological and pathological brain function. *Trends Neurosci.* **36**, 587–597 (2013).
5. Yahaya, T. O. & Salisu, T. F. A Review of Type 2 Diabetes Mellitus Predisposing Genes. *Curr. Diabetes Rev.* **16**, 52–61 (2020).
6. Litwack, G. Glycolysis and Gluconeogenesis. in *Human Biochemistry* 183–198 (2018).
7. Seino, S. Cell signalling in insulin secretion: the molecular targets of ATP, cAMP and sulfonylurea. *Diabetologia* **55**, 2096–2108 (2012).
8. Pilkis, S. J. & Granner, D. K. Molecular Physiology of the Regulation of Hepatic Gluconeogenesis and Glycolysis. *Annu. Rev. Physiol.* **54**, 885–909 (1992).
9. Sims-Robinson, C., Kim, B. & Feldman, E. L. Diabetes and Cognitive Dysfunction. in *Neurobiology of Brain Disorders: Biological Basis of Neurological and Psychiatric Disorders* 189–201 (Elsevier Inc., 2015).
10. Jeker, L. T., Bour-Jordan, H. & Bluestone, J. A. Breakdown in Peripheral Tolerance in Type 1 Diabetes in Mice and Humans. *Cold Spring Harb. Perspect. Med.* **2**, a007807 (2012).
11. CDC. *National Diabetes Statistics Report: Estimates of Diabetes and its Burden in the United States*. (2020).
12. Wood, J. & Peters, A. *The Type 1 Diabetes Self-Care Manual*. *American Diabetes Association* (2018).
13. Riddy, D. M., Delerive, P., Summers, R. J., Sexton, P. M. & Langmead, C. J. G Protein–Coupled Receptors Targeting Insulin Resistance, Obesity, and Type 2 Diabetes Mellitus. *Pharmacol. Rev.* **70**, 39–67 (2018).
14. Nath, S., Ghosh, S. K. & Choudhury, Y. A murine model of type 2 diabetes mellitus developed using a combination of high fat diet and multiple low doses of streptozotocin treatment mimics the metabolic characteristics of type 2 diabetes mellitus in humans. *J. Pharmacol. Toxicol. Methods* **84**, 20–30 (2017).
15. Cohrs, C. M. *et al.* Dysfunction of Persisting β Cells Is a Key Feature of Early Type 2 Diabetes Pathogenesis. *Cell Rep.* **31**, 107469 (2020).
16. Atanes, P. & Persaud, S. J. GPCR targets in type 2 diabetes. in *GPCRs: Structure, Function, and Drug Discovery* 367–391 (Elsevier Inc., 2020).
17. Goldstein, B. J. & Müller-Wieland, D. *Type 2 Diabetes - Principles and Practice, Second Edition*. *Informa Healthcare* (2008).
18. Forbes, J. M. & Cooper, M. E. Mechanisms of Diabetic Complications. *Physiol. Rev.* **93**, 137–

188 (2013).

19. Meldgaard, T. & Brock, C. Diabetes and the gastrointestinal tract. *Medicine (Baltimore).* **47**, 454–459 (2019).

20. Bagyánszki, M. & Bódi, N. Diabetes-related alterations in the enteric nervous system and its microenvironment. *World J. Diabetes* **3**, 80–93 (2012).

21. Tahara, T. & Yamamoto, T. Morphological changes of the villous microvascular architecture and intestinal growth in rats with streptozotocin-induced diabetes. *Virchows Arch. A Pathol. Anat. Histopathol.* **413**, 151–158 (1988).

22. Tomlinson, D. R. & Gardiner, N. J. Glucose neurotoxicity. *Nat. Rev. Neurosci.* **9**, 36–45 (2008).

23. Abbafati, C. *et al.* Global burden of 369 diseases and injuries in 204 countries and territories, 1990–2019: a systematic analysis for the Global Burden of Disease Study 2019. *Lancet* **396**, 1204–1222 (2020).

24. Kirkman, M. S., Briscoe, V. J., Clark, N., Florez, H. & Haas, L. B. Diabetes in Older Adults. *Diabetes Prim. Care* **35**, 2650–2664 (2012).

25. Amati, F. *et al.* Physical Inactivity and Obesity Underlie the Insulin Resistance of Aging. *Diabetes Care* **32**, 1547–1549 (2009).

26. Mangione, C. M. *et al.* Guidelines for Improving the Care of the Older Person with Diabetes Mellitus. *J. Am. Geriatr. Soc.* **51**, S265–S280 (2003).

27. Zheng, Y., Ley, S. H. & Hu, F. B. Global aetiology and epidemiology of type 2 diabetes mellitus and its complications. *Nat. Rev. Endocrinol.* **14**, 88–98 (2018).

28. Cheng, C. Y. *et al.* African Ancestry and Its Correlation to Type 2 Diabetes in African Americans: A Genetic Admixture Analysis in Three U.S. Population Cohorts. *PLoS One* **7**, e32840 (2012).

29. Sickmann, H. M., Waagepetersen, H. S., Schousboe, A., Benie, A. J. & Bouman, S. D. Obesity and type 2 diabetes in rats are associated with altered brain glycogen and amino-acid homeostasis. *J. Cereb. Blood Flow Metab.* **30**, 1527–1537 (2010).

30. Rewers, M. & Ludvigsson, J. Environmental risk factors for type 1 diabetes. *Lancet* **387**, 2340–2348 (2016).

31. Pociot, F. & Lernmark, Å. Genetic risk factors for type 1 diabetes. *Lancet* **387**, 2331–2339 (2016).

32. Pervanidou, P. & Chrousos, G. P. Metabolic consequences of stress during childhood and adolescence. *Metabolism.* **61**, 611–619 (2012).

33. Peterson, L. W. & Artis, D. Intestinal epithelial cells: regulators of barrier function and immune homeostasis. *Nat. Rev. Immunol.* **14**, 141–153 (2014).

34. Johansson, M. E. V. & Hansson, G. C. Immunological aspects of intestinal mucus and mucins. *Nat. Rev. Immunol.* **16**, 639–649 (2016).

35. Gallo, R. L. & Hooper, L. V. Epithelial antimicrobial defence of the skin and intestine. *Nat. Rev. Immunol.* **12**, 503–516 (2012).

36. Gribble, F. M. & Reimann, F. Enteroendocrine Cells: Chemosensors in the Intestinal Epithelium. *Annu. Rev. Physiol.* **78**, 277–299 (2016).

37. Yoo, B. B. & Mazmanian, S. K. The Enteric Network: Interactions between the Immune and Nervous Systems of the Gut. *Immunity* **46**, 910–926 (2017).

38. Margolis, K. G. *et al.* Serotonin transporter variant drives preventable gastrointestinal abnormalities in development and function. *J. Clin. Invest.* **126**, 2221–2235 (2016).

39. Mawe, G. M. & Hoffman, J. M. Serotonin signalling in the gut - functions, dysfunctions and therapeutic targets. *Nat. Rev. Gastroenterol. Hepatol.* **10**, 473–486 (2013).

40. Gribble, F. M. & Reimann, F. Function and mechanisms of enteroendocrine cells and gut hormones in metabolism. *Nat. Rev. Endocrinol.* **15**, 226–237 (2019).

41. Jorsal, T. *et al.* Enteroendocrine K and L cells in healthy and type 2 diabetic individuals. *Diabetologia* **61**, 284–294 (2018).

42. Steinert, R. E. *et al.* Ghrelin, CCK, GLP-1, and PYY(3-36): Secretory Controls and Physiological Roles in Eating and Glycemia in Health, Obesity, and After RYGB. *Physiol. Rev.* **97**, 411–463 (2017).

43. Thompson, E. M., Price, Y. E. & Wright, N. A. Kinetics of enteroendocrine cells with implications for their origin: a study of the cholecystokinin and gastrin subpopulations combining tritiated thymidine labelling with immunocytochemistry in the mouse. *Gut* **31**, 406–411 (1990).

44. Goyal, R. K. & Hirano, I. The Enteric Nervous System. *N. Engl. J. Med.* **334**, 1106–1115 (1996).

45. Wood, J. D. Enteric nervous system. in *Encyclopedia of Gastroenterology* 701–706 (2003).

46. Feher, J. Intestinal and Colonic Chemoreception and Motility. in *Quantitative Human Physiology* 796–809 (2017).

47. Bohórquez, D. V *et al.* Neuroepithelial circuit formed by innervation of sensory enteroendocrine cells. *J. Clin. Invest.* **125**, 782–786 (2015).

48. Bohórquez, D. V. *et al.* An Enteroendocrine Cell - Enteric Glia Connection Revealed by 3D Electron Microscopy. *PLoS One* **9**, e89881 (2014).

49. Fröhlich, F. Synaptic transmission. in *Network Neuroscience* 29–45 (2016).

50. Fon, E. A. & Edwards, R. H. Molecular Mechanisms of Neurotransmitter Release. *Muscle Nerve* **24**, 581–601 (2001).

51. Boto, T. & Tomchik, S. M. The Excitatory, the Inhibitory, and the Modulatory: Mapping Chemical Neurotransmission in the Brain. *Neuron* **101**, 763–765 (2019).

52. Bettler, B., Kaupmann, K., Mosbacher, J. & Gassmann, M. Molecular Structure and Physiological Functions of $GABA_B$ Receptors. *Physiol. Rev.* **84**, 835–867 (2004).

53. Hyland, N. P. & Cryan, J. F. A gut feeling about GABA: focus on $GABA_B$ receptors. *Front. Pharmacol.* **1**, 124–132 (2010).

54. Wang, C., Mao, R., Van De Casteele, M., Pipeleers, D. & Ling, Z. Glucagon-like peptide-1 stimulates GABA formation by pancreatic β-cells at the level of glutamate decarboxylase. *Am. J. Physiol. - Endocrinol. Metab.* **292**, E1201–E1206 (2007).

55. Rorsman, P. *et al.* Glucose-inhibition of glucagon secretion involves activation of $GABA_A$-receptor chloride channels. *Nature* **341**, 233–236 (1989).

56. Shi, Y. *et al.* Increased expression of GAD65 and GABA in pancreatic β-cells impairs first-phase

insulin secretion. *Am. J. Physiol. Endocrinol. Metab.* **279**, E684–E694 (2000).

57. Gu, X. H. *et al.* Suppressive Effect of GABA on Insulin Secretion from the Pancreatic Beta-Cells in the Rat. *Life Sci.* **52**, 687–694 (1993).

58. Ben-Othman, N. *et al.* Long-Term GABA Administration Induces Alpha Cell-Mediated Beta-like Cell Neogenesis. *Cell* **168**, 73-85.e11 (2017).

59. Purwana, I. *et al.* GABA Promotes Human β-Cell Proliferation and Modulates Glucose Homeostasis. *Diabetes* **63**, 4197–4205 (2014).

60. Campagna-Slater, V. & Weaver, D. F. Molecular modelling of the $GABA_A$ ion channel protein. *J. Mol. Graph. Model.* **25**, 721–730 (2007).

61. Taneera, J. *et al.* γ-Aminobutyric acid (GABA) signalling in human pancreatic islets is altered in type 2 diabetes. *Diabetologia* **55**, 1985–1994 (2012).

62. Chua, H. C. & Chebib, M. $GABA_A$ Receptors and the Diversity in their Structure and Pharmacology. in *Ion Channels DownUnder* vol. 79 1–34 (Elsevier Inc., 2017).

63. Santhakumar, V., Wallner, M. & Otis, T. S. Ethanol acts directly on extrasynaptic subtypes of $GABA_A$ receptors to increase tonic inhibition. *Alcohol* **41**, 211–221 (2007).

64. Johnston, G. A. R. $GABA_A$ Receptor Pharmacology. *Pharmacol. Ther.* **69**, 173–198 (1996).

65. Kaupmann, K. *et al.* Expression cloning of $GABA_B$ receptors uncovers similarity to metabotropic glutamate receptors. *Nature* **386**, 239–246 (1997).

66. Gassmann, M. & Bettler, B. Regulation of neuronal $GABA_B$ receptor functions by subunit composition. *Nat. Rev. Neurosci.* **13**, 380–394 (2012).

67. Schwenk, J. *et al.* Modular composition and dynamics of native $GABA_B$ receptors identified by high-resolution proteomics. *Nat. Neurosci.* **19**, 233–242 (2016).

68. Seddik, R. *et al.* Opposite Effects of KCTD Subunit Domains on $GABA_B$ Receptor-mediated Desensitization. *J. Biol. Chem.* **287**, 39869–39877 (2012).

69. Schwenk, J. *et al.* Native $GABA_B$ receptors are heteromultimers with a family of auxiliary subunits. *Nature* **465**, 231–235 (2010).

70. Teng, X. *et al.* KCTD: A new gene family involved in neurodevelopmental and neuropsychiatric disorders. *CNS Neurosci. Ther.* **25**, 887–902 (2019).

71. Metz, M., Gassmann, M., Fakler, B., Schaeren-Wiemers, N. & Bettler, B. Distribution of the Auxiliary $GABA_B$ Receptor Subunits KCTD8, 12, 12b, and 16 in the Mouse Brain. *J. Comp. Neurol.* **519**, 1435–1454 (2011).

72. Skoblov, M. *et al.* Protein partners of KCTD proteins provide insights about their functional roles in cell differentiation and vertebrate development. *BioEssays* **35**, 586–596 (2013).

73. Rajalu, M. *et al.* Pharmacological characterization of $GABA_B$ receptor subtypes assembled with auxiliary KCTD subunits. *Neuropharmacology* **88**, 145–154 (2015).

74. Gastaldelli, A. *et al.* Short-term Effects of Laparoscopic Adjustable Gastric Banding Versus Roux-en-Y Gastric Bypass. *Diabetes Prim. Care* **39**, 1925–1931 (2016).

75. Jørgensen, N. B. *et al.* Acute and long-term effects of Roux-en-Y gastric bypass on glucose metabolism in subjects with Type 2 diabetes and normal glucose tolerance. *Am. J. Physiol. Endocrinol. Metab.* **303**, E122–E131 (2012).

76. Sjostrom, L., Narbro, K. & Sjostrom, C. Effects of Bariatric Surgery on Mortality in Swedish Obese Subjects. *N. Engl. J. Med.* **357**, 741–752 (2007).

77. Sikalidis, A. K. & Maykish, A. The Gut Microbiome and Type 2 Diabetes Mellitus: Discussing a Complex Relationship. *Biomedicines* **8**, 8 (2020).

78. Liou, A. P. *et al.* Conserved Shifts in the Gut Microbiota Due to Gastric Bypass Reduce Host Weight and Adiposity. *Sci. Transl. Med.* **5**, 178ra41 (2013).

79. Kong, L. *et al.* Gut microbiota after gastric bypass in human obesity: increased richness and associations of bacterial genera with adipose tissue genes. *Am. J. Clin. Nutr.* **98**, 16–24 (2013).

80. Rendina-Ruedy, E. *et al.* A Comparative Study of the Metabolic and Skeletal Response of C57BL/6J and C57BL/6N Mice in a Diet-Induced Model of Type 2 Diabetes. *J. Nutr. Metab.* **2015**, 758080 (2015).

81. Kim, B., Kim, Y. Y., Nguyen, P. T.-T., Nam, H. & Suh, J. G. Sex differences in glucose metabolism of streptozotocin-induced diabetes inbred mice (C57BL/6J). *Appl. Biol. Chem.* **63**, 59 (2020).

82. Dinger, K. *et al.* Intraperitoneal Glucose Tolerance Test, Measurement of Lung Function, and Fixation of the Lung to Study the Impact of Obesity and Impaired Metabolism on Pulmonary Outcomes. *J. Vis. Exp.* e56685 (2018).

83. Andrikopoulos, S., Blair, A. R., Deluca, N., Fam, B. C. & Proietto, J. Evaluating the glucose tolerance test in mice. *Am. J. Physiol. - Endocrinol. Metab.* **295**, E1323–E1332 (2008).

84. Scudamore, C. L. *A Practical Guide to the Histology of the Mouse*. *John Wiley & Sons* (2014).

85. Williams, J. M., Duckworth, C. A., Vowell, K., Burkitt, M. D. & Pritchard, D. M. Intestinal Preparation Techniques for Histological Analysis in the Mouse. *Curr. Protoc. Mouse Biol.* **6**, 148–168 (2016).

86. Lee, S. Y. *et al.* Surgical Strategy and Outcomes in Duodenal Gastrointestinal Stromal Tumor. *Ann. Surg. Oncol.* **24**, 202–210 (2017).

87. Aguilar-Nascimento, J. E. De, Salomão, A. B., Nochi Jr., R. J., Nascimento, M. & Neves, J. de S. Intraluminal injection of short chain fatty acids diminishes intestinal mucosa injury in experimental ischemia-reperfusion. *Acta Cirúrgica Bras.* **21**, 21–25 (2006).

88. Fredriksson, S. *et al.* Protein detection using proximity-dependent DNA ligation assays. *Nat. Biotechnol.* **20**, 473–477 (2002).

89. Alam, M. S. Proximity Ligation Assay (PLA). *Curr. Protoc. Immunol.* **123**, e58 (2018).

90. Söderberg, O. *et al.* Direct observation of individual endogenous protein complexes in situ by proximity ligation. *Nat. Methods* **3**, 995–1000 (2006).

91. Odell, I. D. & Cook, D. Immunofluorescence Techniques. *J. Invest. Dermatol.* **133**, e4 (2013).

92. Dunn, K. W., Kamocka, M. M. & McDonald, J. H. A practical guide to evaluating colocalization in biological microscopy. *Am. J. Physiol. Cell Physiol.* **300**, C723–C742 (2011).

93. Sataloff, R. T., Johns, M. M. & Kost, K. M. Colocalisation. *McMaster Biophotonics Facil.* 1–20 (2006).

94. Bolte, S. & Cordelières, F. P. A guided tour into subcellular colocalization analysis in light microscopy. *J. Microsc.* **224**, 213–232 (2006).

95. Bankhead, P. *Analyzing fluorescence microscopy images with ImageJ*. *ImageJ* (2014).

96. Doria, A., Patti, M. E. & Kahn, C. R. The Emerging Genetic Architecture of Type 2 Diabetes. *Cell Metab.* **8**, 186–200 (2008).

97. Bansal, N. Prediabetes diagnosis and treatment: A review. *World J. Diabetes* **6**, 296–303 (2015).

98. Davis, D. B. *et al.* Roux en Y gastric bypass hypoglycemia resolves with gastric feeding or reversal: Confirming a non-pancreatic etiology. *Mol. Metab.* **9**, 15–27 (2018).

99. Zheng, S., Abreu, N., Levitz, J. & Kruse, A. C. Structural basis for KCTD-mediated rapid desensitization of $GABA_B$ signalling. *Nature* **567**, 127–131 (2019).

100. Turecek, R. *et al.* Auxiliary $GABA_B$ receptor subunits uncouple G protein βγ subunits from effector channels to induce desensitization. *Neuron* **82**, 1032–1044 (2014).

101. Pinal, C. S. & Tobin, A. J. Uniqueness and Redundancy in GABA Production. *Perspect. Dev. Neurobiol.* **5**, 109–118 (1998).

102. Kim, J. *et al.* Differential Expression of GAD_{65} and GAD_{67} in Human, Rat, and Mouse Pancreatic Islets. *Diabetes* **42**, 1799–1808 (1993).

103. Towns, R. & Pietropaolo, M. GAD65 autoantibodies and their role as biomarkers of type 1 diabetes and Latent Autoimmune Diabetes in Adults (LADA). *Drugs Future* **36**, 847–854 (2011).

104. Pang, Z. *et al.* Glial fibrillary acidic protein (GFAP) is a novel biomarker for the prediction of autoimmune diabetes. *FASEB J.* **31**, 4053–4063 (2017).

105. Gulbransen, B. D. *Enteric glia*. *Morgan & Claypool* (2014).

106. Grubišić, V. & Gulbransen, B. D. Enteric glia: the most alimentary of all glia. *J. Physiol.* **595**, 557–570 (2016).

107. DiSabato, D. J., Quan, N. & Godbout, J. P. Neuroinflammation: the devil is in the details. *J. Neurochem.* **139**, 136–153 (2016).

108. Craddock, T. J. A. *et al.* A Logic Model of Neuronal-Glial Interaction Suggests Altered Homeostatic Regulation in the Perpetuation of Neuroinflammation. *Front. Cell. Neurosci.* **12**, 336 (2018).

109. Sanada, F. *et al.* Source of Chronic Inflammation in Aging. *Front. Cardiovasc. Med.* **5**, 12 (2018).

110. Franceschi, C. & Campisi, J. Chronic Iinflammation (Inflammaging) and Its Potential Contribution to Age-Associated Diseases. *Journals Gerontol. - Ser. A Biol. Sci. Med. Sci.* **69**, S4–S9 (2014).

111. Gershon, M. D. 5-Hydroxytryptamine (serotonin) in the gastrointestinal tract. *Curr. Opin. Endocrinol. Diabetes. Obes.* **20**, 14–21 (2013).

112. Li, Z. *et al.* Essential Roles of Enteric Neuronal Serotonin in Gastrointestinal Motility and the Development/Survival of Enteric Dopaminergic Neurons. *J. Neurosci.* **31**, 8998–9009 (2011).

113. Gershon, M. D. & Tack, J. The Serotonin Signaling System: From Basic Understanding To Drug Development for Functional GI Disorders. *Gastroenterology* **132**, 397–414 (2007).

114. Charles, K. J., Deuchars, J., Davies, C. H. & Pangalos, M. N. $GABA_B$ receptor subunit expression in glia. *Mol. Cell. Neurosci.* **24**, 214–223 (2003).

115. Meier, S. D., Kafitz, K. W. & Rose, C. R. Developmental Profile and Mechanisms of GABA-Induced Calcium Signaling in Hippocampal Astrocytes. *Glia* **56**, 1127–1137 (2008).

116. Croce, A. C. & Bottiroli, G. Autofluorescence spectroscopy and imaging: A tool for biomedical research and diagnosis. *Eur. J. Histochem.* **58**, 2461 (2014).

117. Qin, W. *et al.* A combined treatment with erythrocyte lysis solution and Sudan Black B reduces tissue autofluorescence in double-labeling immunofluorescence. *Microscopy* **67**, 345–355 (2018).

118. Whittington, N. C. & Wray, S. Suppression of Red Blood Cell Autofluorescence for Immunocytochemistry on Fixed Embryonic Mouse Tissue. *Curr. Protoc. Neurosci.* **81**, 2.28.1-2.28.12 (2017).

6. Appendices

6.1. Tables

Table 6.1: **Commands performed on ImageJ software**, **organized by chronological order**, **and their respective goal**.

Commands	Objective
Image – Lookup Tables – HiLo	Checks for any saturation (red pixels) or background noise
Image – Adjust – Brightness/Contrast…	Enhances the quality of the image by removing saturation and/or background noise
Image – Type – 8-bit	Changes the image type to 8-bit to perform colocalization studies
Image – Color – Merge Channels…	Visual representation of channels in a single image Tick the options "Create composite" and "Keep source images"
Freehand selections	Helps to draw the area corresponding to the lamina propria
Ctrl + M	Gives us the area of the lamina propria
Image – Overlay – To ROI Manager	Saves the drawn area on your software
Open your image(s) of interest and select the ROI drawn	
Image – Adjust – Threshold…	Segments the grayscale images into features of interest
Analyze – Analyze Particles…	Measures features individually “Size (micron^2)” kept at 5-1000 Tick the options "Pixel units", "Display results", "Clear results" and "Add to Manager"
Image – Transform – Image to Results Plugins – Read and Write Excel	Saves the respective results on a Microsoft Excel compatible file
Save the values corresponding to "Area" and "IntDen" (integrated density)	
Repeat the above steps on the other(s) image(s) of interest, if existent	
Oval, elliptical or brush selections	Helps to draw the regions corresponding to background noise
Save the values corresponding to "Mean" (n = 5 background noise measurements)	
Save all images in a TIFF format to keep all the drawn/determined ROI	

Table 6.2: **Colocalization analysis procedure done on ImageJ software**.

Commands	What to select
Select the ROI in one, and only one, of the images of interest	
Analyze – Colocalization – Coloc 2	ImageJ plugin for colocalization analysis
Channel 1 Channel 2	TIFF image with the ROI selected ("green", for example) TIFF image with the ROI not selected ("red", for example)
ROI or Mask	ROI(s) in channel 1
Threshold regression	Bissection (faster and non-dependent of well-equipped workstation computers)
Tick the options "Show Save PDF Dialog" and "Display Images to Result"	
Tick the algorithms "Li Histogram Channel 1", "Li Histogram Channel 2", "Li ICQ" and "2D Intensity Histogram"	
No matter your selection, Pearson's correlation coefficient will always be showcased	

Table 6.3: **Deconvolution analysis performed on Huygens Remote Manager**.

Step	Data input
Number of channels	3
PSF	Theoretical
Microscope type	Widefield
Numerical aperture	1.3
Wavelengths	Excitation [nm]: Ch0: 493; Ch1:353; Ch2: 580 Emission [nm]: Ch0: 517; Ch1:465; Ch2: 618
Objective type	Oil [1.515]
Sample medium	Fluoromount-G™ mounting media with DAPI [1.400]
Voxel size	XY pixel size (nm): 114 Z-step (nm): 300
Time interval (s)	1
Sample orientation	Plane 0 is closest to the coverslip
Correction mode	Perform advanced correction
Deconvolution algorithm	Classic Maximum Likelihood Estimation (CMLE) for all channels
Signal/Noise ratio	40 for all channels
Cropping mode	Do not crop the image
Background mode	Automatic background estimation
Stopping criteria	Number of iterations: 100 Quality change: 0.001
Chromatic aberration correction	Not performed

6.2. Figures

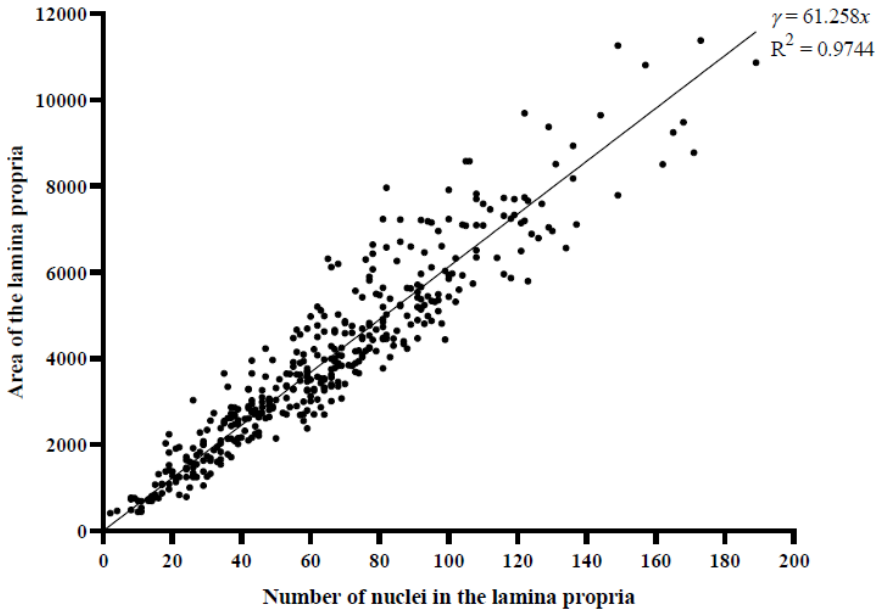

Figure 6.1: **Linear regression analysis showing the relationship between the area of the lamina propria and the number of nuclei within the exact same region**. The area of the lamina propria was determined by selecting the "freehand selections" command on the initial menu of ImageJ, while the number of nuclei was calculated with the help of the "*Oval*, elliptical or brush selections" command, to delineate each one manually as a single ROI. Data were obtained from 416 villi analysed in n = 5 young (208 villi) and n = 5 old C57BL/6J male mice (208 villi).